iScience

CellPress
OPEN ACCESS

Article

MIF-like domain containing protein orchestrates cellular differentiation and virulence in the fungal pathogen *Magnaporthe oryzae*

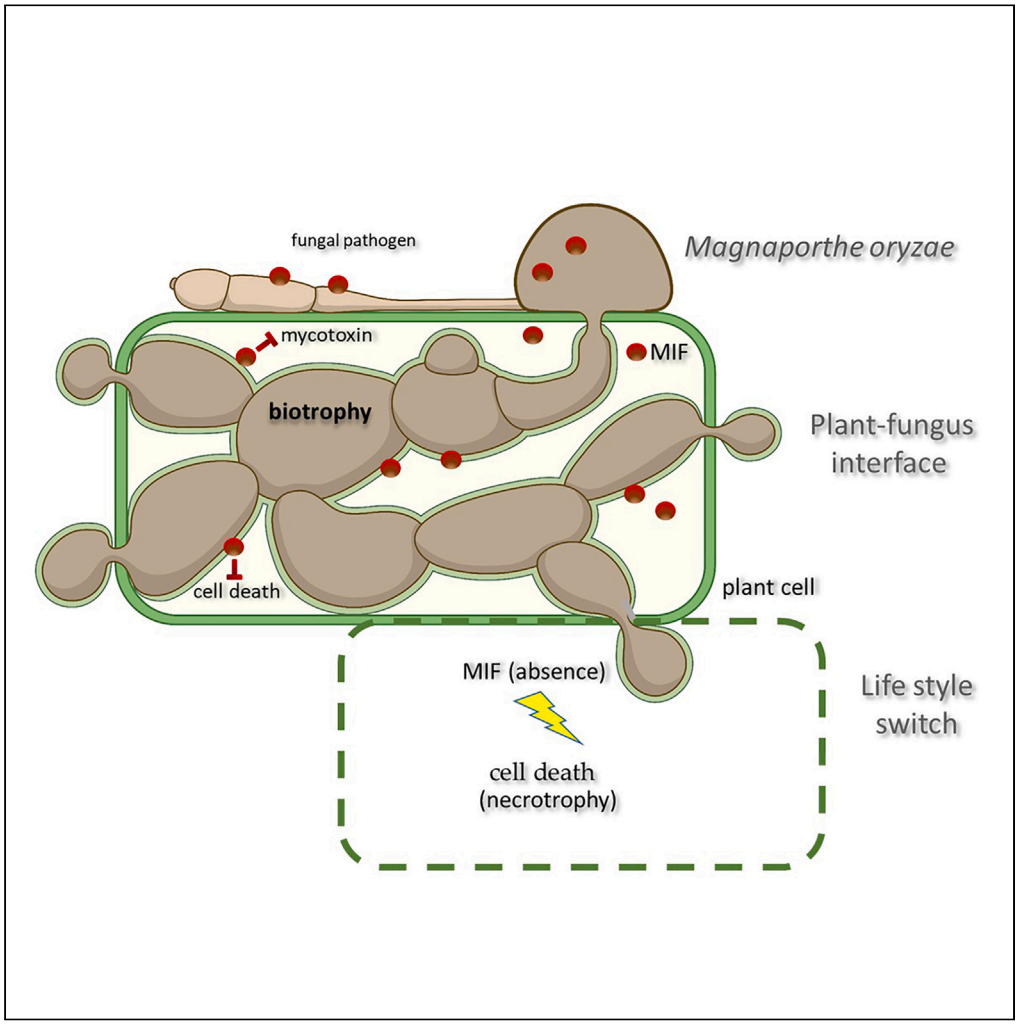

Matteo Galli, Stefan Jacob, Ying Zheng, ..., Harald Keller, Eckhard Thines, Karl-Heinz Kogel

karl-heinz.kogel@agrar.uni-giessen.de

Highlights

Macrophage migration inhibitory factor (MIF1) is a key regulator of fungal virulence

MIF1 maintains the balance between biotrophy and necrotrophy during plant infection

MIF1 affects the production of the mycotoxin tenuazonic acid

MIF1 inhibits plant cell death and is down-regulated in the necrotrophic phase

Galli et al., iScience *26*, 107565
September 15, 2023
https://doi.org/10.1016/j.isci.2023.107565

iScience

CellPress
OPEN ACCESS

Article

MIF-like domain containing protein orchestrates cellular differentiation and virulence in the fungal pathogen *Magnaporthe oryzae*

Matteo Galli,[1,7] Stefan Jacob,[2,7] Ying Zheng,[1] Parviz Ghezellou,[3] Martin Gand,[4] Wendell Albuquerque,[4] Jafargholi Imani,[1] Valérie Allasia,[5] Christine Coustau,[5] Bernhard Spengler,[3] Harald Keller,[5] Eckhard Thines,[2,6] and Karl-Heinz Kogel[1,8,*]

SUMMARY

Macrophage migration inhibitory factor (MIF) is a pleiotropic protein with chemotactic, pro-inflammatory, and growth-promoting activities first discovered in mammals. In parasites, MIF homologs are involved in immune evasion and pathogenesis. Here, we present the first comprehensive analysis of an MIF protein from the devastating plant pathogen *Magnaporthe oryzae* (*Mo*). The fungal genome encodes a single MIF protein (*Mo*MIF1) that, unlike the human homolog, harbors multiple low-complexity regions (LCRs) and is unique to Ascomycota. Following infection, *MoMIF1* is expressed in the biotrophic phase of the fungus, and is strongly down-regulated during subsequent necrotrophic growth in leaves and roots. We show that *Mo*MIF1 is secreted during plant infection, affects the production of the mycotoxin tenuazonic acid and inhibits plant cell death. Our results suggest that *Mo*MIF1 is a novel key regulator of fungal virulence that maintains the balance between biotrophy and necrotrophy during the different phases of fungal infection.

INTRODUCTION

In mammals and plants, cytokines are fundamental mediators of innate immunity and cell signaling.[1–5] They are released after an initial binding of small molecular motifs, such as pathogen-associated molecular patterns (PAMPs), to toll-like receptors (TLRs) or pattern recognition receptors (PRRs).[6,7] Macrophage migration inhibitory factor (MIF) was one of the first cytokines discovered in humans (*Homo sapiens*; *Hs*). Originally, it was related to the delayed-type hypersensitivity reaction, a T-cell-mediated immune response coupled by macrophage activation and infiltration in the inflamed tissue.[8,9] Since then, *Hs*MIF has been associated with a wide range of biological functions, including: *i.* production of other inflammatory cytokines (such as tumor necrosis factor, interleukin-6, interferon-γ, and interleukin-1β), *ii.* hormone immunomodulation, *iii.* regulation of muscle glucose catabolism and other cell metabolic processes, *iv.* tumor growth promotion, *v.* pivotal mediation of immune diseases such as rheumatoid arthritis and atherosclerosis, and *vi.* programmed cell death.[1,10–15] In the human genome, *HsMIF* is located on chromosome 22 and encodes a protein of 114 amino acids (aa). Despite its limited molecular mass, the protein harbors three sequence motifs that confer distinct functional catalytic activities. These include keto-enol tautomerase, thiol-protein oxidoreductase, and DNA nuclease activities.[16–18] *Hs*MIF also acts as a ligand for cell surface receptors such as CD74 and CXCR, thereby triggering multiple signaling pathways underlying the protein's biological functions.[19,20]

A considerable number of *MIF* sequences have been identified in a vast range of organisms across the eukaryotic kingdoms,[21] including nematodes, aphids, protozoans, and mollusks. The genome of the plant model *Arabidopsis thaliana* codes for three distinct MIFs (MIF/D-DT-like proteins, MDLs) and their function has been linked with plant development and modulation of innate immunity.[5] According to current knowledge, MIF in free-living organisms is mainly involved in the activation of immune responses in these species, the proliferation of immune cells and the inhibition of apoptosis mediated by p53.[22–24] However, parasitic species have been shown to produce several MIF proteins, some of which are designated for secretion and to modulate the immune responses in the host organism thus facilitating infection.[25–31] Interestingly MIF proteins do not contain an N-terminal signal sequence and the mechanism of MIF secretion is unclear.[32] Studies on the mode of

[1]Institute of Phytopathology, Research Centre for BioSystems, Land Use and Nutrition, Justus Liebig University Giessen, Heinrich-Buff-Ring 26, 35392 Giessen, Germany
[2]Institute of Biotechnology and Drug Research GmbH, Hanns-Dieter-Hüsch-Weg 17, 55128 Mainz, Germany
[3]Institute of Inorganic and Analytical Chemistry, Justus Liebig University Giessen, Heinrich-Buff-Ring 17, 35392, Giessen, Germany
[4]Institute of Food Chemistry and Food Biotechnology, Justus Liebig University Giessen, Heinrich-Buff-Ring 17, 35392, Giessen, Germany
[5]Université Côte d'Azur, INRAE, CNRS, UMR1355-7254, ISA, 06903 Sophia Antipolis, France
[6]Johannes Gutenberg-University Mainz, Microbiology and Biotechnology at the Institute of Molecular Physiology, Hanns-Dieter-Hüsch-Weg 17, 55128 Mainz, Germany
[7]These authors contributed equally
[8]Lead contact
*Correspondence: karl-heinz.kogel@agrar.uni-giessen.de
https://doi.org/10.1016/j.isci.2023.107565

action and function of such MIF proteins have mainly been conducted on human and plant parasites such as nematodes, protozoa or aphids.[26,30,33,34] Compared to other kingdoms, very little is known about MIF proteins in fungi. Only recently, a comprehensive *in-silico* study about *MIF* evolutionary history in eukaryotes mentioned the fungal MIF protein for the first time.[21] This study showed that fungi possess no or at most one *MIF* sequence in their genome and that the predicted MIF proteins are often associated with other domains. Fungal MIFs therefore appear to be rather unusual cytokines. To elucidate the role of MIF proteins in fungal infection strategies, we studied the filamentous plant pathogen *Magnaporthe oryzae* (*Mo*), the causal agent of devastating blast diseases on many grass species, including the cereals rice, wheat, and barley[35–38]). *Mo* ranks first on the top 10 list of plant pathogenic fungi worldwide.[39] This ascomycete has become a model system for fungi with broad host ranges,[17,40] and for studying the molecular basis of infection-related differentiation processes, including the lifestyle switch from biotrophic to necrotrophic growth that characterizes hemi-biotrophic fungi.[41,42] *Mo* invades plant cells using intracellular invasive hyphae (IHs) that grow from one cell to the next. After penetrating the leaf cuticle from an appressorium, the IH breaches the epidermal cell wall, invaginates the plant plasma membrane, and colonizes the first-invaded cell for 8 to 12 h.[43,44] In this early biotrophic stage of infection, the living host cells are metabolically reprogrammed by fungal effector proteins.[45] Within approximately 48 h post inoculation (hpi), secondary IHs spread into neighboring mesophyll cells, where they are enclosed by a plant membrane, called the extra-invasive hyphal membrane (EIHM). Subsequently, the fungus grows filamentously, and each adjacent plant cell is infected where the cell walls are thinnest (pit field). Newly invaded cells seem to lose their viability when the fungus moves into adjacent ones.[46,47] Of note, fungi of the *Magnaporthe* genus are able to penetrate and colonize cereal roots, resulting in root necrotization. A thorough analysis of the infection strategy of *Magnaporthe grisea* strain Guy11 showed that melanized appressoria associated with classical foliar infection are not required for root infection.[48,49] In contrast, hyphal swellings resembling the simple penetration structures (hyphopodia) of root-infecting fungi were visible at the infection sites. Similar to the early biotrophic growth phase in leaves, the intracellular hyphae are thick and bulbous with constrictions where they cross the plant cell. Here we report the first analysis of a fungal MIF protein and investigate its key function in fungal virulence. We show that the genome of *M. oryzae* harbors one *MIF* gene (*MoMIF1*), which encodes a protein that is unusual in size and structure and differs greatly from MIF homologs in all other taxa, including the closely related Basidiomycota. Using the grass model *Brachypodium distachyon* as host,[50,51] we discovered that *MoMIF1* is expressed in conidia and the very early biotrophic phase but strongly down-regulated in the subsequent necrotrophic phase of plant colonization. Analyses of *MoMIF1* knock-out (KO) and overexpressor (OE) mutants confirmed that *Mo*MIF is detrimental to the necrotrophic phase of fungal development in leaves and roots. Consistent with this, we show that *Mo*MIF1 is a secreted protein with cell death inhibitory activity. Our results suggest that *Mo*MIF1 determines fungal development and virulence by regulating the pathogen's lifestyle switch during infection.

RESULTS

Ascomycota MIFs have unique features

Using the *Hs*MIF gene sequence as reference, we conducted a genome-wide comparison of *MIF* sequences from the EnsemblFungi database.[52] In the subkingdom Dikarya, where most of the plant pathogenic fungi are listed, we found one *MIF*-like gene per genome (Table 1), supporting our previous data on a broad survey of MIF sequences between different kingdoms.[21] Intriguingly, Ascomycota MIFs are much larger proteins (~3 times the size of the *Hs*MIF), compared with MIFs from model organisms of different kingdoms, including Animalia, Plantae, Protozoa and to other Fungi (Figure 1A). The tautomerase/MIF domain motif is located roughly in the middle of the sequence, flanked by long peptide "arms", which carry multiple low complexity regions (LCRs) of unknown function. Phylogenetic analysis with predicted MIF domain sequences from plants, animals, invertebrates and fungi confirmed that Ascomycota MIFs form a separate clade (Figure S1); taking the *Mo*MIF1 domain (MGG_05693) as input sequence, we calculated Ascomycota MIF sequence similarity ranging from 59% to 88%, while Basidiomycota and other taxa MIF domain sequences scored lower (between 50% and 19%; Table 1). Multiple sequence alignment analyses revealed that *Mo*MIF1 lacks CxxCxxHx(n)C (red underlined) and PD-D/E(x)K (green highlighted) motifs, thus suggesting absence of oxidoreductase and DNA nuclease activities, respectively. Furthermore, the active site residues for the tautomerase activity (white triangles) are not conserved (Figure 1B). Moreover, consistent with all MIF proteins identified to date in eukaryotes, *Mo*MIF does not possess a signal peptide for secretion.

*Mo*MIF1 is expressed during conidia germination and appressoria formation

To get a first indication about the requirement of *Mo*MIF for fungal infection, *MoMIF1* expression was recorded in the time range of 0–96 hpi, which covers the biotrophic and the early necrotrophic phase of plant colonization. Leaves of *B. distachyon* Bd21-3 seedlings, which are highly susceptible to *M. oryzae* strain 70-15,[51] were spray-inoculated with conidia and *MoMIF1* expression was measured by RT-qPCR. We detected *MoMIF1* transcripts during the early colonization phase till 12 hpi followed by a steady decline until *MoMIF1* mRNA was almost undetectable between 36 and 42 hpi (Figure 2A). Similarly, upon dip inoculation of roots into a *Mo* spore solution, *MoMIF1* expression was only detected at early infection stages, followed by a decrease in transcript abundance ratio as early as 12–16 hpi (Figure 2B). To further specify the exact timing of accumulation and localization of *Mo*MIF1, we generated a *Mo* reporter strain Δ*Mo*MIF1+GFP that contained a chimeric *MIF1-GFP* gene under the control of the native *MIF1* promoter. Using confocal laser scanning microscopy (CLSM), we examined the pre-infection phase starting with conidia germination on plastic hydrophobic coverslips that are known to induce appressorium formation in *Magnaporthe*.[54,55] Prior to germination, GFP fluorescence was found exclusively in the proximal cell of the three-celled conidia from which the germ tube protrudes, confirming that *MoMIF1* is already expressed in non-germinated conidia. Further analyses over a period of 12 h after conidial germination confirmed accumulation of MIF1-associated fluorescence in both germ tubes and appressoria (Figure 2C). In contrast, *MoMIF1* was not

Table 1. Comparison of the *Mo*MIF1 domain with various eukaryotic MIF domains as identified by species, accession numbers, total protein length, position of the MIF domain in the protein, confidently E-value of the domain and aa similarity to *Mo*MIF1 domainTable

Species	Accession number [Ensembl]	Protein length [aa]	MIF domain position [bp]	MIF domain E-value	MIF domain similarity to *Mo*MIF1
Magnaporthe oryzae[a]	MGG_05693T0	392	164 to 277	2.80E-11	/
Podospora anserina[a]	CAP68549	334	84 to 197	1.20E-12	87.70%
Neurospora crassa[a]	KHE87850	485	171 to 284	7.10E-11	84.20%
Bipolaris oryzae[a]	EUC49493	366	111 to 225	4.90E-16	82.60%
Colletotrichum graminicola[a]	GLRG_03638	373	118 to 232	2.10E-14	81.70%
Erysiphe necator[a]	KHJ30970	335	118 to 231	6.60E-12	78.90%
Verticillium longisporum[a]	CRK39038	692	114 to 226	3.00E-13	78.90%
Microdochium bolleyi[a]	KXJ97725	392	160 to 273	3.00E-11	78.90%
Zymoseptoria tritici[a]	SMQ48239	724	125 to 238	2.80E-16	77.20%
Blumeria graminis f. sp. Tritici[a]	EPQ64960	338	121 to 234	1.10E-10	77.20%
Rhynchosporium commune[a]	CZS95638	338	126 to 238	7.00E-11	75.40%
Rhynchosporium secalis[a]	CZT52938	338	126 to 238	5.10E-11	75.40%
Fusarium graminearum[a]	ESU11401	343	120 to 233	4.90E-10	72.80%
Botrytis cinerea[a]	Bcin10g02580.1	348	138 to 252	1.50E-12	72.20%
Sclerotinia sclerotiorum[a]	APA10581	353	139 to 253	6.60E-12	72.20%
Fusarium culmorum[a]	FCUL_07598.1	343	121 to 233	2.30E-06	71.10%
Trichoderma harzianum[a]	KKO98006	325	106 to 222	5.00E-12	70.90%
Fusarium oxysporum[a]	EWZ34990	338	122 to 233	1.40E-12	69.30%
Sclerotinia borealis[a]	ESZ93718	336	130 to 236	1.20E-11	64.30%
Aspergillus niger[a]	SPB43847	351	137 to 250	1.00E-09	64.00%
Tuber magnatum[a]	PWW80050	330	114 to 226	5.60E-15	62.30%
Tuber borchii[a]	PUU79916	330	114 to 226	3.60E-15	62.30%
Tuber melanosporum[a]	CAZ84338	331	114 to 226	3.60E-17	61.40%
Penicillium digitatum[a]	EKV13723	369	121 to 235	4.40E-10	60.90%
Fonsecaea pedrosoi[a]	KIW84848	326	124 to 236	2.40E-13	60.50%
Verticillium dahliae[a]	EGY14878	335	103 to 206	1.00E-11	60.50%
Exophiala aquamarina[a]	KEF57016	334	131 to 242	1.20E-12	59.60%
Aspergillus oryzae[a]	OOO12748	355	143 to 250	1.90E-07	58.80%
Verticillium alfalfae[a]	EEY22597	340	99 to 206	1.90E-12	58.60%
Phellinus noxius[b]	PAV19534	116	2 to 114	1.40E-23	50.00%
Punctularia strigosozonata[b]	EIN04787	119	2 to 114	1.30E-19	49.60%
Laccaria bicolor[b]	EDR10872	120	2 to 114	1.40E-24	49.10%
Pleurotus ostreatus[b]	KDQ33921	120	2 to 114	3.90E-25	48.20%
Fistulina hepatica[b]	KIY45470	118	2 to 114	3.30E-24	48.20%
Coprinopsis cinerea[b]	EAU88060	124	2 to 119	9.80E-21	45.40%
Daedalea quercina[b]	KZT73998	119	2 to 114	8.00E-21	45.10%
Arabidopsis thaliana #2[c]	AT5G01650.1	115	2 to 115	2.60E-25	44.80%
Caenorhabditis elegans #2[c]	C52E4.2a.1	120	2 to 115	5.10E-52	44.50%
Caenorhabditis elegans #3[c]	F13G3.9.1	146	2 to 113	1.70E-23	44.30%
Galerina marginata[b]	KDR81866	120	2 to 114	3.60E-21	43.00%
Rhizopus microsporus[b]	PHZ17589	122	2 to 114	5.30E-21	43.00%
Homo sapiens[c]	ENST00000215754.8	115	2 to 115	6.40E-55	42.60%
Phytophthora infestans #1[b]	PITG_16205T0	116	2 to 116	6.40E-28	42.00%

(*Continued on next page*)

Table 1. *Continued*

Species	Accession number [Ensembl]	Protein length [aa]	MIF domain position [bp]	MIF domain E-value	MIF domain similarity to *Mo*MIF1
Rhizoctonia solani[b]	EUC66088	123	2 to 117	1.20E-24	40.80%
Plasmodium falciparum[c]	CZT99452	116	2 to 116	3.10E-20	40.50%
Physcomitrium patens[c]	Pp3c13_4090V3.1	115	2 to 115	2.00E-33	40.50%
Grifola frondosa[b]	OBZ75583	123	2 to 109	1.00E-22	40.50%
Phytophthora infestans #2[b]	PITG_16206T0	120	2 to 115	7.30E-25	40.30%
Caenorhabditis elegans #1[c]	Y56A3A.3.1	117	2 to 117	1.10E-28	40.30%
Caenorhabditis elegans #4[c]	Y73B6BL.13.1	121	2 to 117	2.90E-15	39.80%
Mucor ambiguus[b]	GAN02096	118	2 to 114	4.00E-18	39.30%
Arabidopsis thaliana #1[c]	AT5G57170.1	115	2 to 115	1.40E-25	37.40%
Serendipita indica #1[b]	CCA75852	361	9 to 90	1.90E-08	37.10%
Arabidopsis thaliana #3[c]	AT3G51660.1	112	2 to 110	7.10E-13	35.40%
Lichtheimia corymbifera[b]	CDH53730	119	4 to 114	2.10E-15	34.20%
Lichtheimia ramosa[b]	CDS02877	119	5 to 114	2.40E-13	34.10%
Serendipita indica #2[b]	CCA75762	79	1 to 77	1.50E-12	28.00%
Rhizophagus irregularis[b]	PKK71463	88	34 to 88	0.0000005	19.30%

Domain structure comparison via the online-tool SMART with PFAM.[77] Similarity analysis via EMBOSS needle.[78]
[a]Fungus, Ascomycota.
[b]Fungus, non-Ascomycota (Basidiomycota, Oomycota, Mucoromycota, and Glomeromycota.
[c]Other non-fungal organism; aa: amino acid; bp: base pair.

expressed in mycelia from a 5-day-old liquid cultures (Figure 2D). The above data are consistent with the hypothesis that *MoMIF1* is differentially regulated in the bio- and necrotrophic colonization phases and is thus required for successful infection by the hemi-biotrophic fungus.

Both KO and OE of *Mo*MIF1 renders *M. oryzae* less virulent on Bd21-3 leaves

To further explore the function of *Mo*MIF1 during plant infection, we generated knock-out (KO) mutants (Δ*Mo*MIF1-KO_1, Δ*Mo*MIF1-KO_2), overexpressor (OE) mutants (Δ*Mo*MIF1-OE_1, Δ*Mo*MIF1-OE_2), and a complementation mutant Δ*Mo*MIF1-comp (containing *MoMIF1* driven by the original *MIF1* promoter). Southern blot analysis proved the correct manipulation of the fungal genome (Figure S2A), and RT-qPCR analysis confirmed strong *MoMIF1* expression in 5-day-old mycelia of Δ*Mo*MIF1-OE_1 and Δ*Mo*MIF1-OE_2 but not in KO mutants and wild type (WT) (Figure S2B). The KO mutants' germination rate, size, morphology and strength of appressoria measured by the number of appressoria that collapsed after 5 min over a wide range of glycerol concentrations was indistinguishable from the wt (Figure S3A). Moreover, we could not detect substantial differences in mycelium pigmentation, appearance and conidiation on a range of rich (CM) and minimal media (MM) between KO or OE mutants and WT, suggesting that *Mo*MIF1 is dispensable for saprophytic growth (Figure S3B).

The above data together indicated a role of *Mo*MIF1 in the fungal infection process. Therefore, we assessed the virulence of KO and OE mutants on Bd21-3 leaves. Leaves were spray-inoculated and at 5 days post infection (dpi) the total size of the diamond-shaped necrotic blast lesions was recorded. KO mutants elicited significantly smaller necrotic lesions compared to WT (Figures 3A and 3B), and the amount of fungal DNA extracted from infected leaves was significantly lower (Δ*Mo*MIF1-KO_1: 55%; Δ*Mo*MIF1-KO_2: 66% less DNA vs. WT; Figure 3C). Unexpectedly, OE mutants were also strongly impaired in virulence (Δ*Mo*MIF1-OE_1: 79%; Δ*Mo*MIF1-OE_2: 89% reduction in fungal DNA vs. WT), while complementation mutant Δ*Mo*MIF1-comp almost completely restored the WT virulence phenotypes (Figures 3A–3C). Of note, and further supporting the above data, both KO and OE mutants showed also lower virulence on rice (*Oryzae sativa* cv. CO-39) leaves compared with WT (Figure S4). Taken together, our data suggested that the MIF protein of *Mo* is required for virulence and its function is closely linked to the early infection phase, while it seems to have a negative effect on the later necrotrophic development of the fungus.

KO mutants, but not OE mutants heavily colonize Bd21-3 roots

The above assumption prompted us to test the virulence of mutants on Bd21-3 roots. *Mo* penetrates cereal roots without a requirement for appressoria. Tissue colonization is subsequently characterized by a very short biotrophic phase followed by extensive necrotrophic infection.[48,49,56] We thus performed root infection assays to determine whether *Mo*MIF1 is required for root penetration and invasion. Bd21-3 roots from five-day-old seedlings were dip-inoculated with conidia of WT and all mutants. At 5 dpi, roots were carefully removed from the substrate, cleaned, subjected to visual analysis and quantification of fungal DNA. Roots infected with Δ*Mo*MIF1-KO_1 were heavily colonized (Figure 4), were shorter and exhibited more severe root browning compared with WT (Figure S5). In contrast, roots inoculated with Δ*Mo*MIF1-OE_1 showed a slightly reduced necrotization and, consistent with this, colonization was slightly but not significantly reduced as evidenced by lower

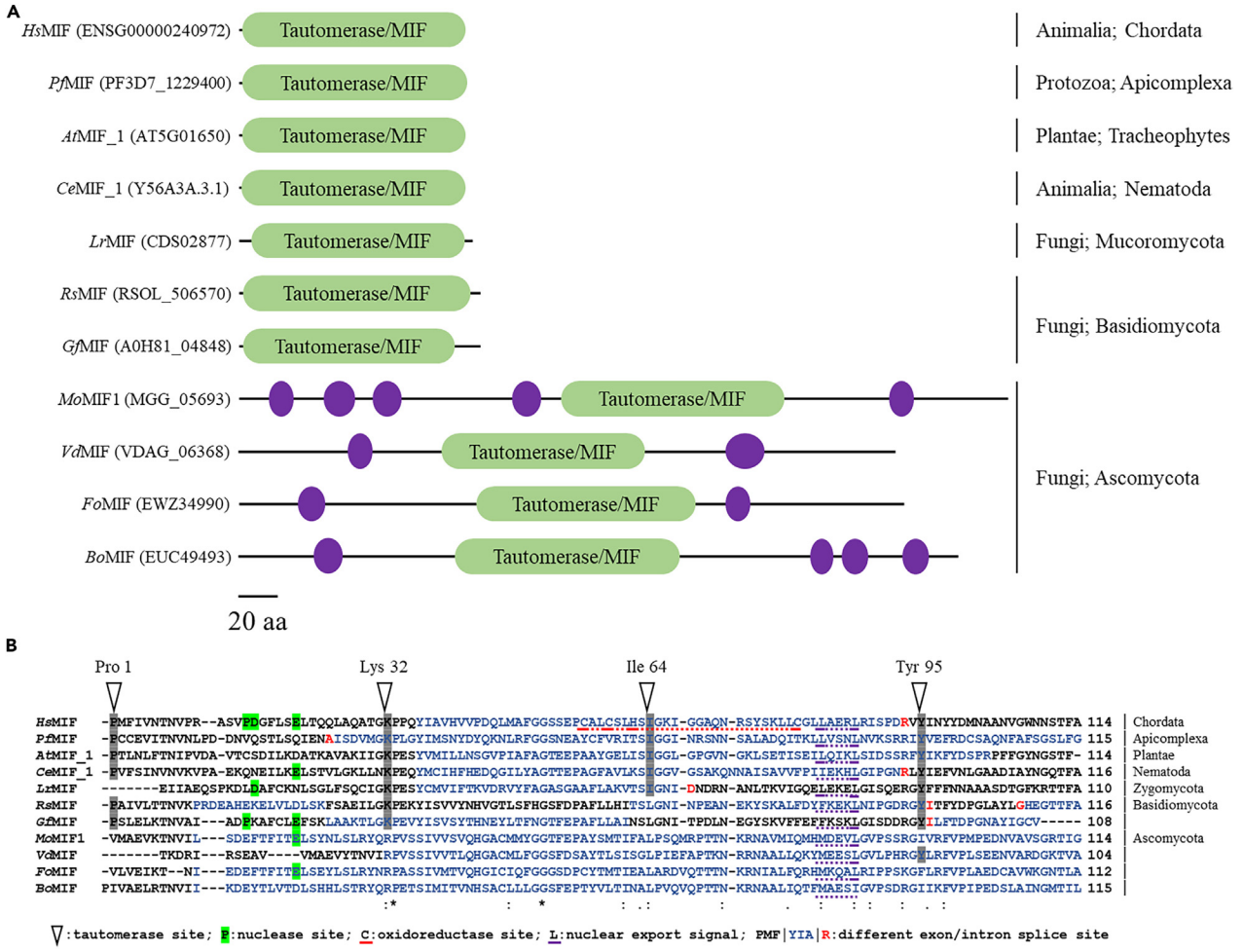

Figure 1. MIF protein domain and structure comparison

(A) Protein organization of *Magnaporthe oryzae* (*Mo*MIF1, MGG_05693) with its homologs in *Homo sapiens* (*Hs*), the protozoan parasite *Plasmodium falciparum* (*Pf*), the genetic plant model organisms *Arabidopsis thaliana* (*At*) and *Caenorhabditis elegans* (*Ce*), one parasitic Mucoromycota fungus *Lichtheimia ramosa* (*Lr*), two plant pathogenic Basidiomycota fungi *Rhizoctonia solani* (*Rs*) and *Grifola frondosa* (*Gf*) and three plant pathogenic Ascomycota fungi *Verticillium dahlia* (*Vd*), *Fusarium oxysporum* (*Fo*) and *Bipolaris oryzae* (*Bo*). Domain structure comparison via the online-tool CDD/SPARCLE.[53] Green marker highlights the Tautomerase/MIF domain, black line represents length of the protein (in scale), and purple circle denotes low complexity region of unknown function.

(B) Conservation of amino acids (aa) sites and motifs in consensus MIF sequences. Hyphens (–) indicate a gap in the respective sequence. Alternance of black and blue color indicates difference exons, red aa indicate that the residue overlaps splice site. Aa sequences marked by symbols (above or below) define distinct functional catalytic activities in human MIF. Tautomerase activity (triangle symbol), oxidoreductase activity (CxxCxxHx(n) motif; red underlined), nuclease activity (PE/DxxxxE motif; green highlighted) and nuclear export signal (LxxxL; purple underlined). Conserved aa residues between species in the tautomerase domain are gray highlighted. Below the protein sequences is a key denoting conserved sequence (*), conservative mutations (), and semi-conservative mutations (.).

amounts of fungal DNA as compared with the WT, while Δ*Mo*MIF1-comp displayed similar root necrotization and infection as the WT (Figures 4; S5). These data further substantiate that i. *Mo*MIF1 is adverse to necrotrophic growth, and that ii. *Mo*MIF1 is not as critical to early root infection as it is to early leaf infection, which is consistent with the knowledge that the biotrophic phase of root invasion is very short followed by extensive necrotrophic infection.

*Mo*MIF1 is detrimental to hyphal expansion into mesophyll cells

The above results are consistent with the idea that *Mo*MIF1 is required at very early stages of fungal infection, while it is rather harmful in later fungal development during necrotizing colonization of plant tissue. To further explore this hypothesis, we injected 100 μL of conidia solution of *MoMIF1* WT and mutants directly into the apoplastic space of second-youngest leaves of three-week-old Bd21-3 seedlings. Injection of conidia circumvents the leaf penetration stage (appressorium-mediated infection and invasion) and shortens the phase of biotrophic growth. We found that injected *MoMIF1* KO mutants were even more virulent than the WT, causing a higher number and larger blast lesions

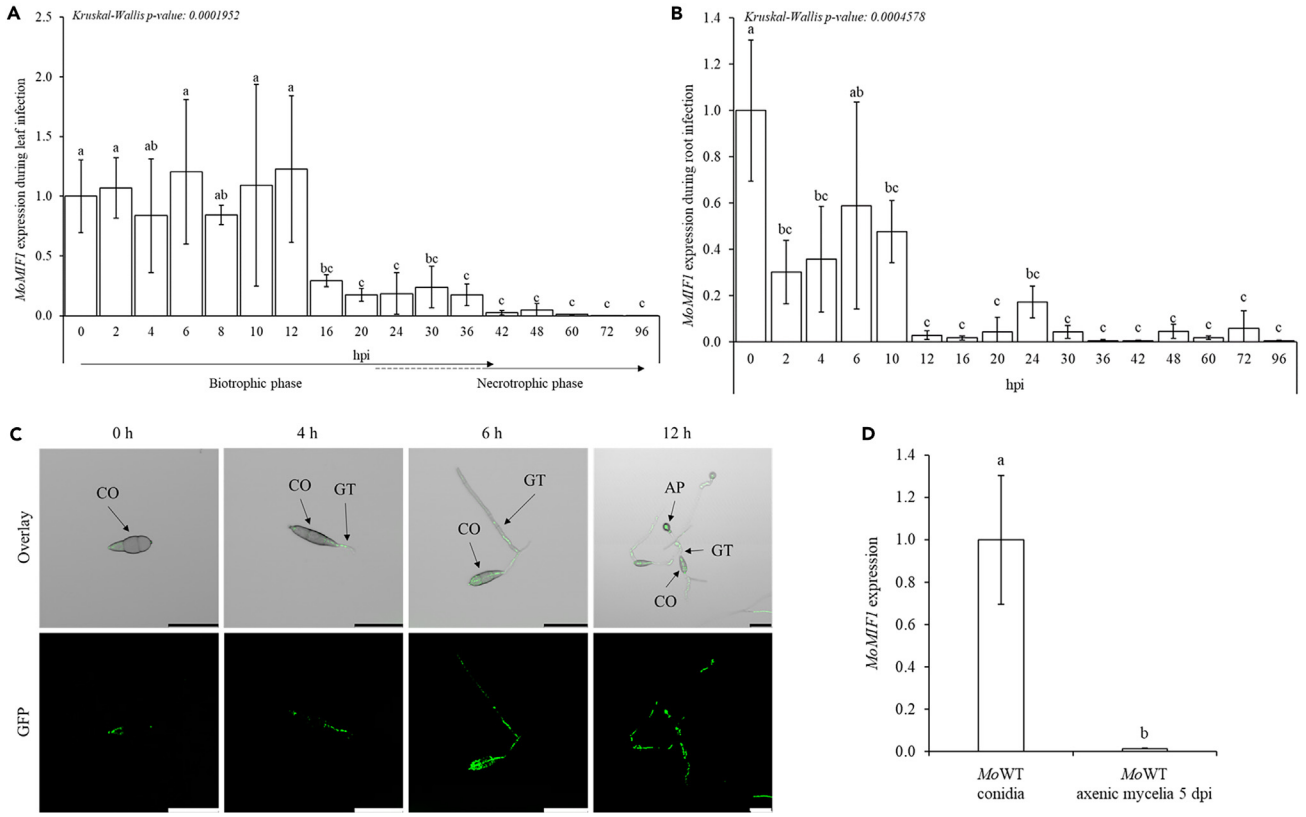

Figure 2. Analysis of *MoMIF1* mRNA and protein localization during *M. oryzae* development

(A and B) Relative *MoMIF1* expression in WT strain 70-15 during fungal development on leaves (a) and roots (b) of the grass model plant *Brachypodium* Bd21-3 as measured by RT-qPCR. Samples were taken from the second youngest spray-inoculated leaf of whole plants (n = 8) and from dip-inoculated roots (n = 6) until 96 hpi, respectively. Inoculum concentration was 120 × 10^3 conidia ml^{-1} in 0.002% Tween 20 water. Fungal *glyceraldehyde-3-phosphate dehydrogenase* (*MoGPD*) was used for normalization. Shown is the mean (±SD) from three biological replicates. Comparisons between groups were performed via Kruskal–Wallis-Test and post hoc pairwise test adjusted with Benjamin-Hochberg correction for multiple comparisons. Letters represent statistical differences among all group means ($\alpha < 0.05$). In the leaf infection graph, time course of the developmental switch during pathogenesis by *Mo* are taken form Parker et al. (2008).[40] The 0 hpi *MoMIF1* expression sample is shared in leaf and root infection.

(C) GFP signals of *Mo*MIF1 C-terminal fused with GFP, detected in germinating Δ*Mo*MIF1+GFP macroconidia (5 × 10^3 mL^{-1} in 0.002% Tween 20) grown on hydrophobic coverslips for 12 h. Scale bar: 100 μm. CO: conidia, GT: germ tube, AP: appressoria; Overlay: GFP: green fluorescence ($\lambda_{emission}$ (nm): 508; $\lambda_{excitation}$ (nm): 489).

(D) RT-qPCR analysis of *MoMIF1* expression in freshly harvested conidia vs. 5-day-old axenic cultures. *MoGPD* was used as normalization gene. Shown is the mean (±SD) from three biological replicates. Comparison between the two groups was performed via pairwise t-tests with Bonferroni's correction. Letters represent statistical differences among group means ($\alpha < 0.05$).

(Figures 5A and 5B). In marked contrast, and consistent with our expectation, injection of *MoMIF1* OE mutants resulted in less infection and substantially reduced necrotic blast symptoms compared to KO mutants (Figures 5A and 5B). Together with the data from root infections, this shows that *Mo*MIF1 is required for the early penetration stage and biotrophic leaf invasion, while it is detrimental to the necrotrophic development of the fungus.

*Mo*MIF1 is a secreted protein

In mammals, insect pests and parasitic protozoa, MIF proteins have been shown to be secreted molecules that enable parasitism and suppress immune responses and cell death, although the exact mechanism of secretion is unclear as no N-terminal signal peptide, nor an internal ER-targeting motifs have been found.[26,30,32,33,57] To determine whether *Mo*MIF1is a secreted protein, we collected intercellular washing fluid (IWF) from WT and *MoMIF* OE mutant-infected leaves at 2 dpi for proteomics analysis. The IWFs were digested in solution with trypsin/lys-C enzymes and the resulting peptides were analyzed by ultra-high-performance liquid chromatography high-resolution tandem mass spectrometry (UHPLC–HR-MS/MS). Four unique peptides were identified with high confidence and confirmed as *Mo*MIF1 protein just in the IWF belonging to Δ*Mo*MIF1-OE_1-infected leaves (Figure S6). On the contrary, no *Mo*MIF1 peptide was detected in the IWFs of WT-infected leaves. The latter is consistent with the low amount of *Mo*MIF1 at the 2 dpi time point as anticipated from its expression profile (see Figure 2A). Importantly, we could not detect any peptides related to broken mycelial remnants (tubulin or actin proteins), suggesting that the *Mo*MIF1

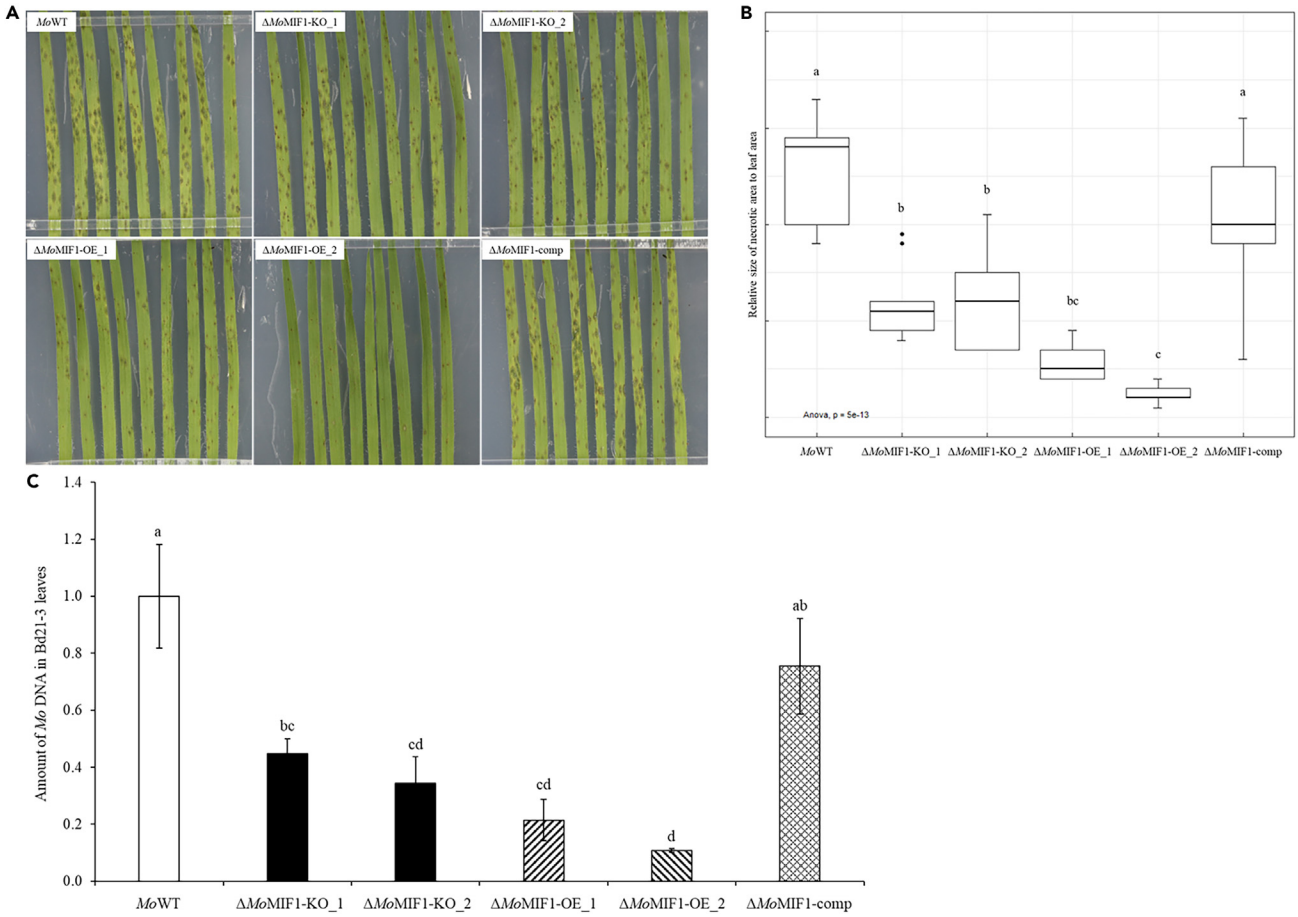

Figure 3. Disease symptoms caused by *Magnaporthe oryzae* 70-15 on *Blm distachyon* Bd21-3 leaves

(A) Phenotypical analysis of the infection phenotypes of WT, *MoMIF1* KO and OE mutants, and complementation mutant Δ*Mo*MIF1-comp. Three-week-old seedlings were sprayed with a suspension of 120 × 10^3 conidia ml^{-1} in 0.002% Tween 20 and kept for 5 days under high humidity at 16 h light/8 h dark cycle at 22°C/18°C.

(B) Size of the necrotic area relative to total leaf size as assayed via ImageJ software at 5 dpi.

(C) Quantification of fungal DNA in second youngest leaves (n = 9 plants) at 5 dpi via qPCR (ratio fungal *GPD* normalized to plant *ubiquitin*). In this experiment two independent KO mutants (Δ*Mo*MIF1-KO_1, Δ*Mo*MIF1-KO_2), and two independent OE mutants (Δ*Mo*MIF1-OE_1, Δ*Mo*MIF1-OE_2) were used. Shown is the mean (±SD) from three biological replicates. Comparisons between groups were performed via ANOVA and Tukey's range test. Letters represent statistical differences among all group means (α = 0.05).

was secreted by the OE mutant during the interaction with the plant. Furthermore, no *Mo*MIF1 peptide was detected in the sterile culture filtrates of either the OE mutants or the WT after 5 dpi, suggesting that *Mo*MIF1 is secreted only when *Mo* is in contact with its host.

*Mo*MIF1 has cell death inhibitory activity

MIF proteins inhibit apoptosis and autophagy-dependent cell death in mammals, insects, and plants.[30,31,58,59] We therefore performed *Agrobacterium*-mediated transient expression assays using leaves of *Nicotiana benthamiana* (*Nb*) to analyze whether *Mo*MIF1 has cell death inhibitory activity. Bcl-2-associated protein X (BAX) activates apoptotic cell death in mammals,[60] which is inhibited by mammalian MIF.[61] Mammalian BAX also triggers hypersensitive response-like cell death in plant tissues upon transient expression of its gene.[62,63] To analyze whether *Mo*MIF1 can inhibit BAX-induced cell death in plants, we performed *Agrobacterium tumefaciens*-mediated transient co-expression experiments in *Nb* leaves (Figure S7). Expression of murine (*Mm*) *BAX* (with *GFP* as control) gave rise to the expected cell death phenotype of the *Agrobacterium*-infiltrated leaf area (top-left half of the leaf), whereas expression of *MoMIF1* (with the *GFP* control) did not affect tissue integrity (bottom-left half of the leaf). Remarkably, when *MmBAX* and *MoMIF1* were simultaneously expressed in the same leaf area, the *Mm*BAX-induced cell death area was clearly and significantly smaller compared to *Mm*BAX alone (right half of the leaf) (Figures S7A,B). These data together suggest that the fungus secretes *Mo*MIF1 to inhibit host cell death during the biotrophic phase of host colonization.

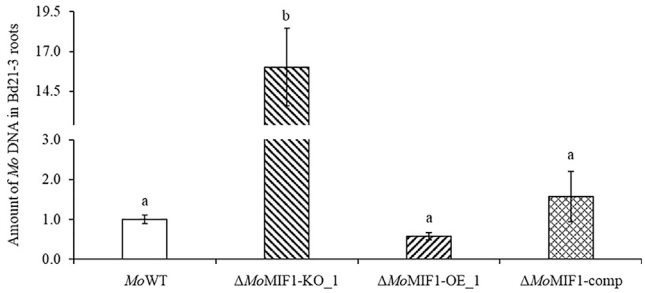

Figure 4. Quantification of fungal DNA in *Brachypodium distachyon* Bd21-3 roots (n = 10 plants) infected with *Mo*WT and MIF mutants at 5 dpi as measured by qPCR based on the ratio of fungal *actin* vs. plant *ubiquitin*

Shown is the mean (±SD) from three biological replicates. Comparisons between' groups were performed via ANOVA and Tukey's Range Test. Letters represent statistical differences among all group means (α = 0.05).'.

*Mo*MIF1 regulates the production of tenuazonic acid

Regulation and fine-tuning of developmental processes are characteristic of chemokines.[64] Studies with animal cells during developmental and pathological processes have revealed links between MIF proteins and the regulation of primary and secondary metabolic processes.[65,66] We therefore tested whether *MoMIF1* WT and KO mutants differ in secondary metabolite production. Chemical analysis by means of HPLC and HPLC-MS revealed that the KO mutants produced increased amounts of tenuazonic acid (TeA), independent of the nature of the culture medium, whereas the WT produces only traces thereof (Figures 6A and 6B). TeA is a well-known non-host selective mycotoxin that inhibits protein biosynthesis at the ribosome by suppressing the release of new proteins. It is particularly important for the establishment of infection by many necrotrophic fungi, such as those from the genera *Alternaria* and *Phoma* that secrete (TeA), thereby causing ROS production necroses and cell death in infected leaves.[67,68] Overall, these results are consistent with the notion that *Mo*MIF1 is a negative regulator of TeA production, suggesting a scenario in which transient *Mo*MIF1 expression at early infection stages inhibits the mycotoxin production during the biotrophic phase, while subsequent downregulation of *Mo*MIF1 de-represses its production in the necrotrophic phase.

DISCUSSION

Based on a survey of MIF homologues in the kingdom Fungi (EnsemblFungi database,[52] we discovered that members of the monophyletic group Ascomycota carry atypical MIF proteins, which are unique to this phylum (Table 1; Figure S1). Compared to the closer phyla Mucoromycota, Zoopagomycota, Glomeromycota, and Basidiomycota, which harbor typical MIF proteins, Ascomycota carry larger MIFs, in which the tautomerase domain is flanked by long peptide "arms" (Figure 1A). Similarly, the marine dinoflagellate *Lingulodinium polyedrum* (*Lp*) from the phylum Myzozoa (infrakingdom Alveolata) also produces an atypical MIF protein.[69] *Lp*MIF (246 aa) is a transmembrane-anchored MIF protein with an extracytoplasmic MIF domain associated with vesicle bodies, cell wall and extracellular vesicles.[69] The presence of related sequences in such disparate phyla suggests that selective pressure has influenced the evolution of the MIF protein scaffold to meet different physiological needs. In Ascomycota, this hypothesis is specially backed by the presence of several LCR motifs with unknown function flanking the tautomerase/MIF domain (Figure 1A). Experimental and computational evidence increasingly suggests that LCRs have adaptive and conserved roles in protein evolution.[70–72] In particular, they may contribute to protein conformational plasticity therefore broadening the range of interacting molecules.[70] A recent study shows that the localization of VAMP-associated protein (VAP-A) to different membrane contact sites (MCSs) in human cells depends on its LCRs.[73] VAP-A also enables lipid exchange at ER-Golgi MCSs by interacting with oxysterol-binding protein (OSBP) and Ceramide Transfer Protein (CERT), while removing LCRs from VAP-A restricts its distribution and function to ER-mitochondria MCS. Thus, LCR-mediated conformational protein flexibility ensures membrane tethering plasticity and efficiency. It is tempting to speculate that *Mo*MIF participates in early steps of pathogenicity through supporting focal interaction at the fungus - host interface.

We discovered that a fungal MIF is a highly regulated gene whose activity rather strictly correlates with the two parasitic life stages of the hemibiotrophic fungus *M. oryzae*, with transcripts accumulating in conidia and the early germination/penetration phase of biotrophic growth and dropping off sharply as it enters necrotrophic growth on the host plant (Figure 2A). Remarkably, there is very little gene expression detected in the necrotrophic growth phase, neither in the infected leaf nor in the root tissue. As we found that the *Mo*MIF has cell death inhibitory activity (Figure S7), it is plausible that the presence of *Mo*MIF in this host-cell death associated phase[48,49] would be detrimental to fungal development and virulence. Thus, our data together suggest that accumulation of *Mo*MIF1 is required at stages where the pathogenic fungus is confronted with the very early host immune response, i.e., during the attachment and colonization of the host surface and during the biotrophy-associated growth within the first leaf cell, where it functions as cell death inhibitor and negative regulator of the mycotoxin TeA, thus keeping host cells alive (Figures 6A and 6B). The detection of *Mo*MIF1 in IWFs at an early stage of plant infection (Figure S6) further supports this scenario. However, further experiments are required to accurately determine the location of the *Mo*MIF protein at specific time points of infection. This is necessary to rule out the possibility that the biphasic activity of the molecule correlates with differential cellular compartmentalization, i.e., during the early time points of germination and penetration its activity in the fungal cell might dampen tenuazonic acid production, while it then becomes secreted for cell death repression.

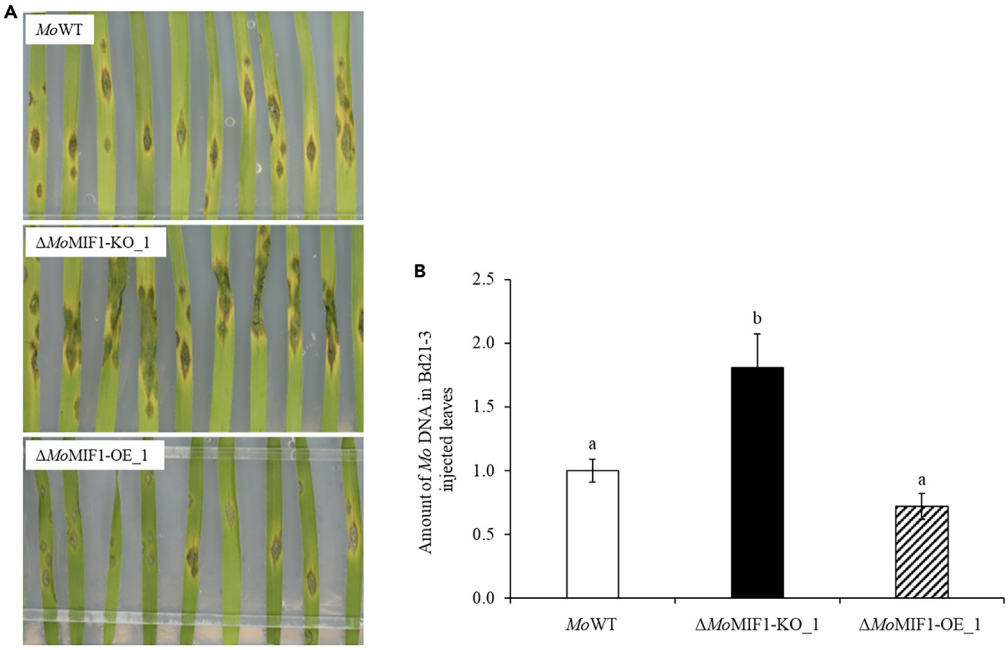

Figure 5. Disease symptoms caused by injection of *Mo* conidia into the apoplastic space of Bd21€-3

(A) Phenotypical analysis of the injection infection phenotypes of WT, *MoMIF1* KO and OE mutants. The second youngest leaf of three-week-old seedlings (n = 8 plants) were injected with a suspension of 120 × 10^3 conidia ml^{-1} in 0.002% Tween 20 and kept for 5 days under high humidity at 16 h light/8 h dark cycle at 22°C/18°C.

(B) Quantification of fungal DNA at 5 dpi via qPCR (ratio fungal *GPD* normalized to plant *ubiquitin*). Shown is the mean (±SD) from three biological replicates. Comparisons between' groups were performed via ANOVA and Tukey's Range Test. Letters represent statistical differences among all group means (α = 0.05).

In-planta experiments with fungal mutants carrying aberrant *MIF1* genes further highlighted the importance of a strict and fine-tuned regulation of *MoMIF1* expression for the development of the typical blast symptoms as both KO and OE mutants are strongly attenuated in virulence (Figures 2; 3A–3C; S4). Excitingly, bypassing the appressorium-mediated entry and biotrophic epidermal cell invasion by injecting *Mo* conidia directly into the mesophyll apoplastic space, rendered KO mutants highly aggressive, while higher amounts of *Mo*MIF1 in *MoMIF1* OE mutants reduced the spread of infection (Figure 4; S5; 5A and 5B), unambiguously demonstrating that *Mo*MIF activity is detrimental to fungal virulence in the necrotrophic phase.

Mo secretes effector proteins and structurally distinct secondary metabolites into the host to suppress plant immunity, manipulate the biological activities and finally kill the plant cell.[47,74,75] We discovered that *Mo*MIF1 is a negative regulator of tenuazonic acid, a host cell death-inducing mycotoxin secreted by necrotrophic fungi such as those from the genus Alternaria and Phoma,[67,68] and which has also been described previously in the genus Magnaporthe.[76] Interestingly, the latter authors reported the cell death-inducing activity of TeA in plants, but also that exogenous TeA reduces the fitness of the fungus. This shows that tight control of TeA biosynthesis is essential for fungal survival.

Taken together, our findings are consistent with the view that in plant pathogenic organisms MIF proteins are important regulators of host cell death that serve to prolong parasitism and plant exploitation.[30,31,58,59] *Mo* produces and secretes the atypical MIF1 protein to influence the infection life cycle of the pathogen through activities on both the fungus itself (metabolic reprogramming) and host plant cells (inhibition of cell death). We suggest that the protein contributes to the maintenance of biotrophy of the hemibiotrophic fungus, in analogy to what has been found for MIF activities in mammals and invertebrates. However, further experiments are needed to confirm whether the orthologous domain of MIF from Ascomycota could complement the function of the human MIF domain.

Limitations of the study

Our study focused on the contribution of a novel MIF to the virulence of the fungal ascomycete pathogen *M. oryzae* on its host plants. Biochemical analysis of the novel protein, including the mode of action of the different MIF domains and their functionality, was not in the focus of our research. In addition, we investigated the presence (biotrophy) and absence (necrotrophy) of the *Mo*MIF by quantification of gene expression, and did not include further quantification methods. We did not quantify a high or low expression of the basal expression level of *MoMIF* at time 0, but were interested in quantifying the relative difference of gene expression in the two different lifestyle phases of the colonizing fungus, where we found a strong downshift in the necrotrophic phase. Finally, the information on the molecular mechanism of

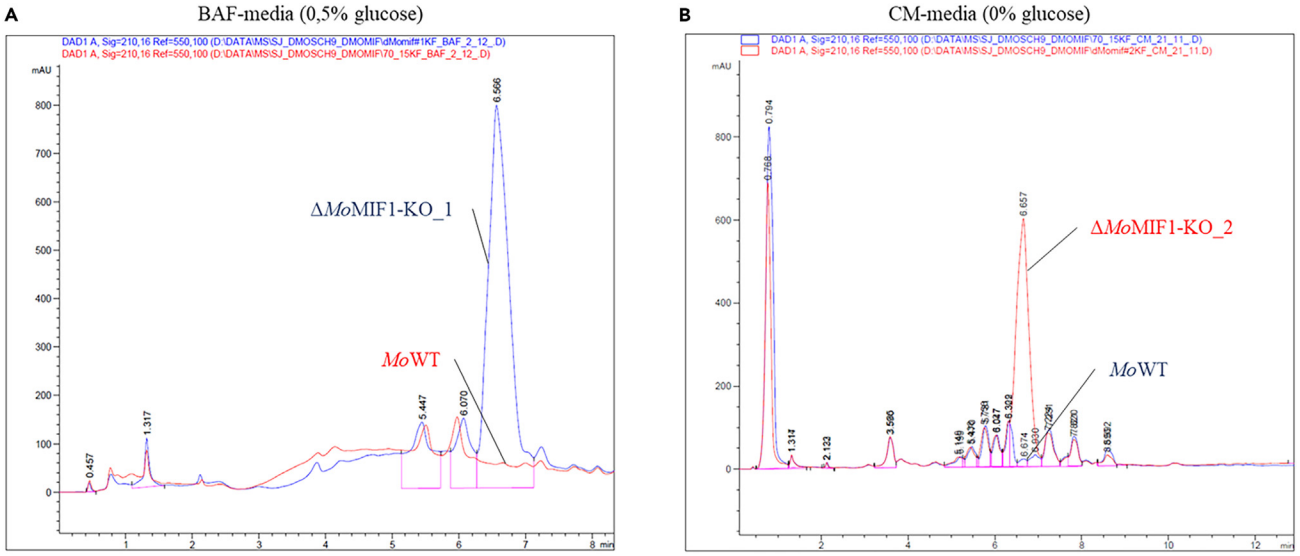

Figure 6. Quantification of tenuazonic acid (TeA) in *Mo*WT and MIF1 mutants. HPLC-MS analysis of metabolites extracted from WT and the KO mutant Δ*Mo*MIF1-KO_1 and Δ*Mo*MIF1-KO_2 in BAF medium plus 0.5% Glucose (A) or CM (B)

The indicated peaks mark the TeA area. Each strain was submerged-cultured for 5 days at 25°C in axenic cultures. The experiment was repeated three times with similar results.

*Mo*MIF secretion and compartmentalization in the different phases of fungal lifestyle is limited as it is not in the focus of this work. This study should be understood as the first analysis of a fungal MIF focusing on the non-canonical *MIF* gene in Ascomycota.

STAR★METHODS

Detailed methods are provided in the online version of this paper and include the following:

- KEY RESOURCES TABLE
- RESOURCE AVAILABILITY
  - Lead contact
  - Materials availability
  - Data and code availability
- EXPERIMENTAL MODEL AND STUDY PARTICIPANT DETAILS
  - Plant cultivars and fungal strain
- METHOD DETAILS
  - Fungal inoculation protocols
  - DNA manipulations and construction of fungal transformation vectors
  - Protein organization comparison and phylogenetic analysis
  - Production of sterile crude extracts from *Mo* cultures and IWF from *Mo*-infected Bd21-3 leaves
  - HPLC/MS method for analysis of secondary fungal metabolites
  - Protein purification and bottom-up proteomics analysis
  - Vegetative growth assays
  - Appressorium formation assays and conidia morphology
  - Confocal laser scanning microscopy
  - Transient expression in *N. benthamiana*
- QUANTIFICATION AND STATISTICAL ANALYSIS
  - DNA/RNA isolation and quantitative PCR and RT-PCR analysis
  - Statistical analysis

SUPPLEMENTAL INFORMATION

Supplemental information can be found online at https://doi.org/10.1016/j.isci.2023.107565.

ACKNOWLEDGMENTS

We thank Christina Birkenstock and Martina Claar for their excellent technical support. This work was carried out within the framework of the German/French cooperation program by the Deutsche Forschungsgemeinschaft (DFG) and the Agence Nationale de la Recherche (ANR) through project numbers Ko 1208/25-1 (KHK) and ANR-16-CE92-0014-01 (C.C. and H.K.), through the "Investments for the Future" LABEX SIGNALIFE: program reference ANR-11-LABX-0028-01 (C.C. and H.K.). P.G. and B.S. acknowledge financial support by DFG (INST 162/500-1 FUGG) and by the State of Hesse through LOEWE Center DRUID (Novel Drug Targets against Poverty-Related and Neglected Tropical Infectious Diseases). Y.Z. was supported by German Academic Exchange Service (DAAD).

AUTHOR CONTRIBUTIONS

K.H.K., M.G., H.K., and S.J. wrote the manuscript; K.H.K., E.T., M.G., S.J., H.K., C.C., and M.G. designed the study; M.G., Y.Z., J.I., V.A., P.G., and W.A. prepared material for the experiments; K.H.K., C.C., E.T., and B.S. provided methodology and instrumentation; M.G., Y.Z., J.I., V.A., P.G., and W.A. conducted the experiments; M.G., S.J., E.T., C.C., P.G., H.K., B.S., and K.H.K. analyzed all data and drafted the figures. All authors commented and reviewed the final manuscript.

DECLARATION OF INTERESTS

The authors declare no competing interests.

Received: August 6, 2022
Revised: May 20, 2023
Accepted: August 3, 2023
Published: August 6, 2023

REFERENCES

1. Calandra, T., and Roger, T. (2003). Macrophage migration inhibitory factor: a regulator of innate immunity. Nat. Rev. Immunol. *3*, 791–800.
2. Choi, J., Huh, S.U., Kojima, M., Sakakibara, H., Paek, K.H., and Hwang, I. (2010). The cytokinin-activated transcription factor ARR2 promotes plant immunity via TGA3/NPR1-dependent salicylic acid signaling in Arabidopsis. Dev. Cell *19*, 284–295.
3. Merk, M., Mitchell, R.A., Endres, S., and Bucala, R. (2012). D-dopachrome tautomerase (D-DT or MIF-2): doubling the MIF cytokine family. Cytokine *59*, 10–17.
4. Panstruga, R., Baumgarten, K., and Bernhagen, J. (2015). Phylogeny and evolution of plant macrophage migration inhibitory factor/D-dopachrome tautomerase-like proteins. BMC Evol. Biol. *15*, 64.
5. Gruner, K., Leissing, F., Sinitski, D., Thieron, H., Axstmann, C., Baumgarten, K., Reinstädler, A., Winkler, P., Altmann, M., Flatley, A., et al. (2021). Chemokine-like MDL proteins modulate flowering time and innate immunity in plants. J. Biol. Chem. *296*, 100611.
6. Akira, S., and Hemmi, H. (2003). Recognition of pathogen-associated molecular patterns by TLR family. Immunol. Lett. *85*, 85–95.
7. Ausubel, F.M. (2005). Are innate immune signaling pathways in plants and animals conserved? Nat. Immunol. *6*, 973–979.
8. Bloom, B.R., and Bennett, B. (1966). Mechanism of a reaction in vitro associated with delayed-type hypersensitivity. Science *153*, 80–82.
9. David, J.R. (1966). Delayed hypersensitivity in vitro: its mediation by cell-free substances formed by lymphoid cell-antigen interaction. Proc. Natl. Acad. Sci. USA. *56*, 72–77.
10. Takahashi, N., Nishihira, J., Sato, Y., Kondo, M., Ogawa, H., Ohshima, T., Une, Y., and Todo, S. (1998). Involvement of macrophage migration inhibitory factor (MIF) in the mechanism of tumor cell growth. Mol. Med. *4*, 707–714.
11. Fingerle-Rowson, G., Petrenko, O., Metz, C.N., Forsthuber, T.G., Mitchell, R., Huss, R., Moll, U., Müller, W., and Bucala, R. (2003). The p53-dependent effects of macrophage migration inhibitory factor revealed by gene targeting. Proc. Natl. Acad. Sci. USA. *100*, 9354–9359.
12. Onodera, S., Nishihira, J., Koyama, Y., Majima, T., Aoki, Y., Ichiyama, H., Ishibashi, T., and Minami, A. (2004). Macrophage migration inhibitory factor up-regulates the expression of interleukin-8 messenger RNA in synovial fibroblasts of rheumatoid arthritis patients: Common transcriptional regulatory mechanism between interleukin-8 and interleukin-1β. Arthritis Rheum. *50*, 1437–1447.
13. Morand, E.F., Leech, M., and Bernhagen, J. (2006). MIF: a new cytokine link between rheumatoid arthritis and atherosclerosis. Nat. Rev. Drug Discov. *5*, 399–410.
14. Bifulco, C., McDaniel, K., Leng, L., and Bucala, R. (2008). Tumor growth-promoting properties of macrophage migration inhibitory factor. Curr. Pharm. Des. *14*, 3790–3801.
15. Wang, Y., An, R., Umanah, G.K., Park, H., Nambiar, K., Eacker, S.M., Kim, B., Bao, L., Harraz, M.M., Chang, C., et al. (2016). A nuclease that mediates cell death induced by DNA damage and poly (ADP-ribose) polymerase-1. Science *354*, aad6872.
16. Rosengren, E., Åman, P., Thelin, S., Hansson, C., Ahlfors, S., Björk, P., Jacobsson, L., and Rorsman, H. (1997). The macrophage migration inhibitory factor MIF is a phenylpyruvate tautomerase. FEBS Lett. *417*, 85–88.
17. Routledge, A.P.M., Shelley, G., Smith, J.V., Talbot, N.J., Draper, J., and Mur, L.A.J. (2004). *Magnaporthe grisea* interactions with the model grass *Brachypodium distachyon* closely resemble those with rice (*Oryza sativa*). Mol. Plant Pathol. *5*, 253–265.
18. Kleemann, R., Kapurniotu, A., Frank, R.W., Gessner, A., Mischke, R., Flieger, O., Jüttner, S., Brunner, H., and Bernhagen, J. (1998). Disulfide analysis reveals a role for macrophage migration inhibitory factor (MIF) as thiol-protein oxidoreductase. J. Mol. Biol. *280*, 85–102.
19. Shi, X., Leng, L., Wang, T., Wang, W., Du, X., Li, J., McDonald, C., Chen, Z., Murphy, J.W., Lolis, E., et al. (2006). CD44 is the signaling component of the macrophage migration inhibitory factor-CD74 receptor complex. Immunity *25*, 595–606.
20. Tillmann, S., Bernhagen, J., and Noels, H. (2013). Arrest functions of the MIF ligand/receptor axes in atherogenesis. Front. Immunol. *4*, 115.
21. Mitchell, R.A., Liao, H., Chesney, J., Fingerle-Rowson, G., Baugh, J., David, J., and Bucala, R. (2002). Macrophage migration inhibitory factor (MIF) sustains macrophage proinflammatory function by inhibiting p53: regulatory role in the innate immune response. Proc. Natl. Acad. Sci. USA. *99*, 345–350.
22. Jung, H., Seong, H.A., and Ha, H. (2008). Critical role of cysteine residue 81 of macrophage migration inhibitory factor (MIF) in MIF-induced inhibition of p53 activity. J. Biol. Chem. *283*, 20383–20396.
23. Baeza-Garcia, A., Pierce, R.J., Gourbal, B., Werkmeister, E., Colinet, D., Reichhart, J.M., Dissous, C., and Coustau, C. (2010). Involvement of the cytokine MIF in the snail host immune response to the parasite *Schistosoma mansoni*. PLoS Pathog. *6*, e1001115.
24. Brock, S.E., Rendon, B.E., Xin, D., Yaddanapudi, K., and Mitchell, R.A. (2014). MIF family members cooperatively inhibit p53 expression and activity. PLoS One *9*, e99795.

25. Pastrana, D.V., Raghavan, N., FitzGerald, P., Eisinger, S.W., Metz, C., Bucala, R., Schleimer, R.P., Bickel, C., and Scott, A.L. (1998). Filarial nematode parasites secrete a homologue of the human cytokine macrophage migration inhibitory factor. Infect. Immun. *66*, 5955–5963.
26. Augustijn, K.D., Kleemann, R., Thompson, J., Kooistra, T., Crawford, C.E., Reece, S.E., Pain, A., Siebum, A.H.G., Janse, C.J., and Waters, A.P. (2007). Functional characterization of the *Plasmodium falciparum* and *P. berghei* homologues of macrophage migration inhibitory factor. Infect. Immun. *75*, 1116–1128.
27. Cho, Y., Vermeire, J.J., Merkel, J.S., Leng, L., Du, X., Bucala, R., Cappello, M., and Lolis, E. (2011). Drug repositioning and pharmacophore identification in the discovery of hookworm MIF inhibitors. Chem. Biol. *18*, 1089–1101.
28. Miller, J.L., Harupa, A., Kappe, S.H.I., and Mikolajczak, S.A. (2012). *Plasmodium yoelii* macrophage migration inhibitory factor is necessary for efficient liver-stage development. Infect. Immun. *80*, 1399–1407.
29. Ajonina-Ekoti, I., Kurosinski, M.A., Younis, A.E., Ndjonka, D., Tanyi, M.K., Achukwi, M., Eisenbarth, A., Ajonina, C., Lüersen, K., Breloer, M., et al. (2013). Comparative analysis of macrophage migration inhibitory factors (MIFs) from the parasitic nematode *Onchocerca volvulus* and the free-living nematode *Caenorhabditis elegans*. Parasitol. Res. *112*, 3335–3346.
30. Naessens, E., Dubreuil, G., Giordanengo, P., Baron, O.L., Minet-Kebdani, N., Keller, H., and Coustau, C. (2015). A secreted MIF cytokine enables aphid feeding and represses plant immune responses. Curr. Biol. *25*, 1898–1903.
31. Zhao, J., Li, L., Liu, Q., Liu, P., Li, S., Yang, D., Chen, Y., Pagnotta, S., Favery, B., Abad, P., and Jian, H. (2019). A MIF-like effector suppresses plant immunity and facilitates nematode parasitism by interacting with plant annexins. J. Exp. Bot. *70*, 5943–5958.
32. Flieger, O., Engling, A., Bucala, R., Lue, H., Nickel, W., and Bernhagen, J. (2003). Regulated secretion of macrophage migration inhibitory factor is mediated by a non-classical pathway involving an ABC transporter. FEBS Lett. *551*, 78–86.
33. Vermeire, J.J., Cho, Y., Lolis, E., Bucala, R., and Cappello, M. (2008). Orthologs of macrophage migration inhibitory factor from parasitic nematodes. Trends Parasitol. *24*, 355–363.
34. Liu, S., Ladera-Carmona, M.J., Poranen, M.M., van Bel, A.J.E., Kogel, K.H., and Imani, J. (2021). Evaluation of dsRNA delivery methods for targeting macrophage migration inhibitory factor MIF in RNAi-based aphid control. J. Plant Dis. Prot. *128*, 1201–1212.
35. Urashima, A.S., Lavorent, N.A., Goulart, A.C.P., and Mehta, Y.R. (2004). Resistance spectra of wheat cultivars and virulence diversity of *Magnaporthe grisea* isolates in Brazil. Fitopatol. Bras. *29*, 511–518.
36. Ebbole, D.J. (2007). Magnaporthe as a model for understanding host-pathogen interactions. Annu. Rev. Phytopathol. *45*, 437–456.
37. Faivre-Rampant, O., Thomas, J., Allègre, M., Morel, J.B., Tharreau, D., Nottéghem, J.L., Lebrun, M.H., Schaffrath, U., and Piffanelli, P. (2008). Characterization of the model system rice-Magnaporthe for the study of nonhost resistance in cereals. New Phytol. *180*, 899–910.
38. Cruz, C.D., Bockus, W.W., Stack, J.P., Tang, X., Valent, B., Pedley, K.F., and Peterson, G.L. (2012). Preliminary assessment of resistance among US wheat cultivars to the Triticum pathotype of *Magnaporthe oryzae*. *Plant Disease*. Plant Dis. *96*, 1501–1505.
39. Dean, R., Van Kan, J.A.L., Pretorius, Z.A., Hammond-Kosack, K.E., Di Pietro, A., Spanu, P.D., Rudd, J.J., Dickman, M., Kahmann, R., Ellis, J., and Foster, G.D. (2012). The Top 10 fungal pathogens in molecular plant pathology. Mol. Plant Pathol. *13*, 414–430.
40. Parker, D., Beckmann, M., Enot, D.P., Overy, D.P., Rios, Z.C., Gilbert, M., Talbot, N., and Draper, J. (2008). Rice blast infection of *Brachypodium distachyon* as a model system to study dynamic host/pathogen interactions. Nat. Protoc. *3*, 435–445.
41. Yan, X., and Talbot, N.J. (2016). Investigating the cell biology of plant infection by the rice blast fungus *Magnaporthe oryzae*. *Curr. Opin. Microbiol*. Curr. Opin. Microbiol. *34*, 147–153.
42. Fernandez, J., and Orth, K. (2018). Rise of a cereal killer: the biology of *Magnaporthe oryzae* biotrophic growth. Trends Microbiol. *26*, 582–597.
43. Martin-Urdiroz, M., Oses-Ruiz, M., Ryder, L.S., and Talbot, N.J. (2016). Investigating the biology of plant infection by the rice blast fungus *Magnaporthe oryzae*. *Fungal Genet. Biol*. Fungal Genet. Biol. *90*, 61–68.
44. Zhu, J., Jeong, J.S., and Khang, C.H. (2021). Tandem DNA repeats contain cis-regulatory sequences that activate biotrophy-specific expression of Magnaporthe effector gene PWL2. Mol. Plant Pathol. *22*, 508–521.
45. Giraldo, M.C., Dagdas, Y.F., Gupta, Y.K., Mentlak, T.A., Yi, M., Martinez-Rocha, A.L., Saitoh, H., Terauchi, R., Talbot, N.J., and Valent, B. (2013). Two distinct secretion systems facilitate tissue invasion by the rice blast fungus *Magnaporthe oryzae*. Nat. Comm *4*, 1–12.
46. Kankanala, P., Czymmek, K., and Valent, B. (2007). Roles for rice membrane dynamics and plasmodesmata during biotrophic invasion by the blast fungus. Plant Cell *19*, 706–724.
47. Wilson, R.A., and Talbot, N.J. (2009). Under pressure: investigating the biology of plant infection by *Magnaporthe oryzae*. *Nat. Rev. Microbiol*. Nat. Rev. Microbiol. *7*, 185–195.
48. Sesma, A., and Osbourn, A.E. (2004). The rice leaf blast pathogen undergoes developmental processes typical of root-infecting fungi. Nature *431*, 582–586.
49. Tucker, S.L., Besi, M.I., Galhano, R., Franceschetti, M., Goetz, S., Lenhert, S., Osbourn, A., and Sesma, A. (2010). Common genetic pathways regulate organ-specific infection-related development in the rice blast fungus. Plant Cell *22*, 953–972.
50. Scholthof, K.B.G., Irigoyen, S., Catalan, P., and Mandadi, K.K. (2018). Brachypodium: a monocot grass model genus for plant biology. Plant Cell *30*, 1673–1694.
51. Zanini, S., Šečić, E., Busche, T., Galli, M., Zheng, Y., Kalinowski, J., and Kogel, K.H. (2021). Comparative Analysis of Transcriptome and sRNAs Expression Patterns in the *Brachypodium distachyon-Magnaporthe oryzae* Pathosystems. Int. J. Mol. Sci. *22*, 650.
52. Howe, K.L., Contreras-Moreira, B., De Silva, N., Maslen, G., Akanni, W., Allen, J., Alvarez-Jarreta, J., Barba, M., Bolser, D.M., Cambell, L., et al. (2020). Ensembl Genomes 2020-enabling non-vertebrate genomic research. Nucleic Acids Res. *48*, 689–695.
53. Marchler-Bauer, A., Bo, Y., Han, L., He, J., Lanczycki, C.J., Lu, S., Chitsaz, F., Derbyshire, M.K., Geer, R.C., Gonzales, N.R., et al. (2017). CDD/SPARCLE: functional classification of proteins via subfamily domain architectures. Nucleic Acids Res. *45*, 200–203.
54. Yong-Hwan Lee, R., and Dean, R.A. (1994). Hydrophobicity of contact surface induces appressorium formation in *Magnaporthe grisea*. FEMS Microbiol. Lett. *115*, 71–75.
55. Thines, E., Weber, R.W., and Talbot, N.J. (2000). MAP kinase and protein kinase A-dependent mobilization of triacylglycerol and glycogen during appressorium turgor generation by *Magnaporthe grisea*. *Plant Cell*. Plant Cell *12*, 1703–1718.
56. Marcel, S., Sawers, R., Oakeley, E., Angliker, H., and Paszkowski, U. (2010). Tissue-adapted invasion strategies of the rice blast fungus *Magnaporthe oryzae*. *Plant Cell*. Plant Cell *22*, 3177–3187.
57. Bernhagen, J., Mitchell, R.A., Calandra, T., Voelter, W., Cerami, A., and Bucala, R. (1994). Purification, bioactivity, and secondary structure analysis of mouse and human macrophage migration inhibitory factor (MIF). Biochemistry *33*, 14144–14155.
58. Balogh, K.N., Templeton, D.J., and Cross, J.V. (2018). Macrophage Migration Inhibitory Factor protects cancer cells from immunogenic cell death and impairs anti-tumor immune responses. PLoS One *13*, e0197702.
59. Zhao, M., Chang, Q., Liu, Y., Sang, P., Kang, Z., and Wang, X. (2021). Functional characterization of the wheat Macrophage Migration Inhibitory Factor TaMIF1 in wheat-stripe rust (*Puccinia striiformis*) interaction. Biology *10*, 878.
60. Boise, L.H., Gottschalk, A.R., Quintáns, J., and Thompson, C.B. (1995). Bcl-2 and Bcl-2-related proteins in apoptosis regulation. Curr. Top. Microbiol. Immunol. *200*, 107–121.
61. Baumann, R., Casaulta, C., Simon, D., Conus, S., Yousefi, S., and Simon, H.U. (2003). Macrophage migration inhibitory factor delays apoptosis in neutrophils by inhibiting the mitochondria-dependent death pathway. FASEB J *17*, 2221–2230.
62. Lacomme, C., and Santa Cruz, S. (1999). Bax-induced cell death in tobacco is similar to the hypersensitive response. Proc. Natl. Acad. Sci. USA. *96*, 7956–7961.
63. Hückelhoven, R., Dechert, C., and Kogel, K.H. (2003). Overexpression of barley BAX inhibitor 1 induces breakdown of mlo-mediated penetration resistance to *Blumeria graminis*. Proc. Natl. Acad. Sci. *100*, 5555–5560.
64. Bromley, S.K., Mempel, T.R., and Luster, A.D. (2008). Orchestrating the orchestrators: chemokines in control of T cell traffic. Nat. Immunol. *9*, 970–980.
65. Serre-Beinier, V., Toso, C., Morel, P., Gonelle-Gispert, C., Veyrat-Durebex, C., Rohner-Jeanrenaud, F., Calandra, T., Roger, T., James, R.W., Montet, X., et al. (2010). Macrophage migration inhibitory factor deficiency leads to age-dependent impairment of glucose homeostasis in mice. J. Endocrinol. *206*, 297–306.
66. Michelet, C., Danchin, E.G.J., Jaouannet, M., Bernhagen, J., Panstruga, R., Kogel, K.H., Keller, H., and Coustau, C. (2019). Cross-kingdom analysis of diversity, evolutionary history, and site selection within the

eukaryotic macrophage migration inhibitory factor superfamily. Genes *10*, 740.
67. Yun, C.S., Motoyama, T., and Osada, H. (2015). Biosynthesis of the mycotoxin tenuazonic acid by a fungal NRPS–PKS hybrid enzyme. Nat. Commun. *6*, 8758–8759.
68. Shi, J., Zhang, M., Gao, L., Yang, Q., Kalaji, H.M., Qiang, S., Strasser, R.J., and Chen, S. (2021). Tenuazonic acid-triggered cell death is the essential prerequisite for *Alternaria alternata* (Fr.) Keissler to infect successfully host *Ageratina adenophora*. *Cells*. Cells *10*, 1010.
69. Jaouannet, M., Pavaux, A.S., Pagnotta, S., Pierre, O., Michelet, C., Marro, S., Keller, H., Lemée, R., and Coustau, C. (2020). Atypical Membrane-Anchored Cytokine MIF in a Marine Dinoflagellate. Microorganisms *8*, 1263.
70. Ntountoumi, C., Vlastaridis, P., Mossialos, D., Stathopoulos, C., Iliopoulos, I., Promponas, V., Oliver, S.G., and Amoutzias, G.D. (2019). Low complexity regions in the proteins of prokaryotes perform important functional roles and are highly conserved. Nucleic Acids Res. *47*, 9998–10009.
71. Mier, P., Paladin, L., Tamana, S., Petrosian, S., Hajdu-Soltész, B., Urbanek, A., Gruca, A., Plewczynski, D., Grynberg, M., Bernadó, P., et al. (2020). Disentangling the complexity of low complexity proteins. Brief. Bioinform. *21*, 458–472.
72. Dickson, Z.W., and Golding, G.B. (2022). Low complexity regions in mammalian proteins are associated with low protein abundance and high transcript abundance. Mol. Biol. Evol. *39*, msac087.
73. Subra, M., Dezi, M., Bigay, J., Lacas-Gervais, S., Di Cicco, A., Araújo, A.R.D., Abélanet, S., Fleuriot, L., Debayle, D., Gautier, R., et al. (2023). VAP-A intrinsically disordered regions enable versatile tethering at membrane contact sites. Dev. Cell *58*, 121–138.e9.
74. Collemare, J., Billard, A., Böhnert, H.U., and Lebrun, M.H. (2008). Biosynthesis of secondary metabolites in the rice blast fungus *Magnaporthe grisea*: the role of hybrid PKS-NRPS in pathogenicity. Mycol. Res. *112*, 207–215.
75. Thines, E., Anke, H., and Weber, R.W.S. (2004). Fungal secondary metabolites as inhibitors of infection-related morphogenesis in phytopathogenic fungi. Mycol. Res. *108*, 14–25.
76. Aver'yanov, A.A., Lapikova, V.P., and Lebrun, M.H. (2007). Tenuazonic acid, toxin of rice blast fungus, induces disease resistance and reactive oxygen production in plants. Russ. J. Plant Physiol. *54*, 49–754.
77. Letunic, I., Khedkar, S., and Bork, P. (2021). SMART: recent updates, new developments and status in 2020. Nucleic Acids Res. *49*, D458–D460.
78. Needleman, S.B., and Wunsch, C.D. (1970). A general method applicable to the search for similarities in the amino acid sequence of two proteins. J. Mol. Biol. *48*, 443–453.
79. Vogel, J., and Hill, T. (2008). High-efficiency Agrobacterium-mediated transformation of *Brachypodium distachyon* inbred line Bd21-3. Plant Cell Rep. *27*, 471–478.
80. Odenbach, D., Breth, B., Thines, E., Weber, R.W.S., Anke, H., and Foster, A.J. (2007). The transcription factor Con7p is a central regulator of infection-related morphogenesis in the rice blast fungus Magnaporthe grisea. Mol. Microbiol. *64*, 293–307.
81. Bohnert, S., Neumann, H., Thines, E., and Jacob, S. (2019). Visualizing fungicide action: an in vivo tool for rapid validation of fungicides with target location HOG pathway. Pest Manag. Sci. *75*, 772–778.
82. Edgar, R.C. (2004). MUSCLE: a multiple sequence alignment method with reduced time and space complexity. BMC Bioinf. *5*, 113–119.
83. Le, S.Q., and Gascuel, O. (2008). An improved general amino acid replacement matrix. Mol. Biol. Evol. *25*, 1307–1320.
84. Kumar, S., Stecher, G., Li, M., Knyaz, C., and Tamura, K. (2018). MEGA X: molecular evolutionary genetics analysis across computing platforms. Mol. Biol. Evol. *35*, 1547–1549.
85. Pogorelko, G., Fursova, O., Lin, M., Pyle, E., Jass, J., and Zabotina, O.A. (2011). Post-synthetic modification of plant cell walls by expression of microbial hydrolases in the apoplast. Plant Mol. Biol. *77*, 433–445.
86. Ghezellou, P., Albuquerque, W., Garikapati, V., Casewell, N.R., Kazemi, S.M., Ghassempour, A., and Spengler, B. (2021). Integrating top-down and bottom-up mass spectrometric strategies for proteomic profiling of iranian saw-scaled viper, echis carinatus sochureki, venom. J. Prot. Res. *20*, 895–908.
87. Sowa, M.A., Kreuter, N., Sella, N., Albuquerque, W., Manhard, J., Siegl, A., Ghezellou, P., Li, B., Spengler, B., Weichhard, E., et al. (2022). Replacement of pregastric lipases in cheese production: identification and heterologous expression of alLipase from *Pleurotus citrinopileatus*. *J. Agric. Food Chem*. J. Agric. Food Chem. *70*, 2998–3008.
88. Jacob, S., Foster, A.J., Yemelin, A., and Thines, E. (2014). Histidine kinases mediate differentiation, stress response, and pathogenicity in *Magnaporthe oryzae*. *Microbiologyopen*. Microbiologyopen *3*, 668–687.
89. Gilbert, R.D., Johnson, A.M., and Dean, R.A. (1996). Chemical signals responsible for appressorium formation in the rice blast fungus *Magnaporthe grisea*. *Physiol. Mol. Plant Pathol*. Physiol. Mol. Plant Pathol. *48*, 335–346.
90. Kumar, N., Galli, M., Ordon, J., Stuttmann, J., Kogel, K.H., and Imani, J. (2018). Further analysis of barley MORC 1 using a highly efficient RNA-guided Cas9 gene-editing system. Plant Biotechnol. J. *16*, 1892–1903.

STAR★METHODS

KEY RESOURCES TABLE

REAGENT or RESOURCE	SOURCE	IDENTIFIER
Fungal strains		
Δ*Mo*MIF1-KO	This paper	N/A
Δ*Mo*MIF1-OE	This paper	N/A
Δ*Mo*MIF1-GFP	This paper	N/A
Δ*Mo*MIF1-comp	This paper	N/A
Chemicals, peptides, and recombinant proteins		
Tenuazonic acid	Cayman Chemicals	Item no. 11443
Deposited data		
Ensembl	EMBL-EBI	N/A
Software and algorithms		
ImageJ	https://imagej.nih.gov/ij/	N/A
Leica LAS X software	https://www.leica-microsystems.com/products/microscope-software/p/leica-las-x-ls/downloads/	N/A
Other		
HPLC-MS (Agilent 1260 Series LC and 6130 Series Quadrupole MS System)	N/A	N/A

RESOURCE AVAILABILITY

Lead contact

Further information and requests for resources and reagents should be directed to and will be fulfilled by the Lead Contact, Prof. Dr. Karl-Heinz Kogel (Karl-Heinz.Kogel@agrar.uni-giessen.de).

Materials availability

There are restrictions to the availability of plasmids and reagent due to the limited amount of the original stocks. Direct inquiries regarding plasmids and reagent generated as part of this study should be directed to the Lead Contact, Prof. Dr. Karl-Heinz Kogel (Karl-Heinz.Kogel@agrar.uni-giessen.de).

Data and code availability

All data generated or analyzed during this study are included in this published article [and its supplementary information files].

EXPERIMENTAL MODEL AND STUDY PARTICIPANT DETAILS

Plant cultivars and fungal strain

The fungal strain used in this study was *Magnaporthe oryzae* strain 70-15 strain (Fungal Genetics Stock Center, Kansas State University, Manhattan, USA). The strain was grown at 26°C on Complete medium (CM; pH 6.5, 2% agar, containing per liter 10 g glucose, 1 g yeast extract, 2 g peptone, 1 g casamino acids, 50 mL nitrate salt solution [120 g NaNO3, 10.4 g KCl, 30.4 g KH2PO4, 10.4 g MgSO4 x 7 H2O per liter] and 1 mL of a trace element solution [22 g ZnSO4 x 7 H2O, 11 g H3BO3, 5 g MnCl2 x 4 H2O, 5 g FeSO4 x 7 H2O, 1.7 g CoCl2 x 6 H2O, 1.6 g CuSO4 x 5 H2O, 1.5 g Na2MoO4 x 2 H2O and 50 g Na2EDTA, pH 6.5 adjusted by 1 M KOH per liter]. Minimal medium (MM; pH 6.5) contains 1 g glucose, 0.25 mL of a 0.01% biotin solution, 50 mL nitrate salt solution, 1 mL of a trace element solution, and 1 mL of a 1% thiamine dichloride solution per liter.

The plants cultivars used in this study were *Brachypodium distachyon* and *Oryzae sativa*. *Brachypodium distachyon* cv. Bd21-3[79] was cultivated in soil (Fruhstorfer Erde Typ T, Vechta, Germany) in a growth chamber at 22°C/18°C (day/night cycle) with 60% relative humidity and a photoperiod of 240 μmol m^{-2} s^{-1} photon flux density.

Dwarf indica rice cultivar CO-39 was cultivated using a daily cycle of 16 h/8 h light/dark (28°C, 80% relative humidity). Depending on the experiments, plants in different developmental stage were used ranging from one to three week-old. For more precise information see the method description in the next paragraph.

METHOD DETAILS

Fungal inoculation protocols

For plant inoculation, *Mo* conidia were used. Germination of conidia and appressoria development were assessed by incubating a suspension of 5 x 10^3 conidia ml^{-1} in double distilled water on plastic coverslips (Sigma-Aldrich, Saint Louis, USA) in a damp chamber at room temperature using an inverted microscopy. Two methods were used to assess disease progression of *Mo* strains in plant leaves: *i.* Leaf-spray inoculation of three-week-old Bd21-3 plants with a suspension of 120 x 10^3 ml^{-1} conidia in 0.002% v/v Tween20 until water run-off; *ii.* injection of 100 µl of the above suspension into the apoplastic space of second youngest intact leaves of three-week-old Bd21-3 using a syringe. Tenuazonic acid (TeA, copper salt, Cayman Chemical Company, Michigan, USA) was used at a concentration of 5 mM in double distilled H_2O (TeA first resuspension in 0.5% v/v DMSO). Control seedlings were mock-inoculated with 0.002% v/v Tween20 water in all setups. Disease progression and analysis of the necrotic spots were assayed at 5 dpi via ImageJ software. For rice infection, conidial suspensions were adjusted to 5 x 10^4 conidia ml^{-1} in H_2O containing 0.2% gelatin. Five 21-day-ol rice plants were spray inoculated each with 5 mL of conidial suspension and incubated in plastic bags in a test chamber (Versatile Environmental Test Chamber MLR-350H; Sanyo Electric Co., Illinois, USA). For root inoculation, Bd21-3 seeds were surface sterilized with a solution of 3% v/v NaClO for 15 min, followed by three times 5 min washes in sterile water, before being placed on half-strength MS medium in 16 h light (160 µmol m^{-2} s^{-1})/8 h dark cycle at 22°C/18°C. Roots of one-week-old seedlings were dip-inoculated in 1 ml of conidial suspension (120 x 10^3 ml^{-1} in 0.002% v/v Tween20) for 3 h and later transplanted in vermiculite (Deutsche Vermiculite GmbH, Sprockhövel, Germany). Control roots were mock inoculated with 1 ml 0.002% v/v Tween20.

DNA manipulations and construction of fungal transformation vectors

The DNA of *Mo* 70–15 was isolated from mycelia of 3-day-old liquid cultures (grown in CM at 26°C and 100 rpm) using the DNeasy® plant mini Kit (Qiagen GmbH, Hilden, Germany), following the manufacturer's instructions for purification of DNA from plants and filamentous fungi. The DNA manipulation followed standard procedures. *Escherichia coli* XL1-BLUE strain (Stratagene) or NEB® 10-ß Competent *Escherichia coli* strains (High Efficiency) were used for routine bacterial transformations and the construction of plasmids. Transformation of *Mo* was conducted using *Agrobacterium tumefaciens*-mediated transformation (ATMT). The detailed procedures followed those described in Odenbach et al. (2007).[80]

To generate the MIF1 loss-of-function mutants Δ*Mo*MIF1-KO_1 and Δ*Mo*MIF1-KO_2, the coding gene sequence of *MoMIF1* (MGG_05693) was completely replaced by the HPT gene from *pSJ-basic* (IBWF-73, Bohnert et al., 2019), using the Gibson Assembly® cloning method. The flanking regions (1000 bp) of *MoMIF* were amplified by PCR from genomic DNA with primers SJ-1249/SJ-1250 and SJ-1253/SJ-1254. The *HPT* gene was amplified from *pSJ+basic* using the primer SJ-1251/SJ-1252. The backbone vector was a *PstI/BglII*-restricted *pSJ-basic*. The 7,917 bp plasmid *pSJ-MIF-HPT* was used to transform WT via ATMT, resulting in the mutant strain Δ*Mo*MIF1-KO_1 and Δ*Mo*MIF1-KO_2.

For the fluorescence marked strain Δ*Mo*MIF1+GFP, we used a two-step cloning strategy. We initially generated the plasmid *pSJ+flank1+EF1+GFP+BAR+flank2*. Therefore, the plasmid *pSJ+GFP(BAR)*[81] was used as template to amplify fragment *EF1+GFP+BAR* using the primer pair SJ-1628/SJ-1629. Fragment 1 is generated in order to obtain a strong expression of the *eGFP*-gene, so the *EF1α*-promoter of *Mo* (gene MGG_03641) was cloned N-terminal of the *eGFP* gene, which was originally amplified from *pEGFP-1* (BD Biosciences). At the C-terminal end of the *eGFP* sequence, the *NOS*-terminator was inserted, directly followed by the *BAR* sequence.[81] The flanking regions (500 bp) of *MoMIF1* were amplified by PCR from genomic DNA with primers SJ-1626/SJ-1627 and SJ-1630/SJ-1631. The backbone vector was a *PstI/BglII*-restricted *pSJ-basic*. The resulting 8,562 bp plasmid *pSJ+flank1+EF1+GFP+BAR+flank2* was then used as backbone to insert the MIF coding sequence in the *NcoI* restriction site between *EF1* and *GFP*. The MIF fragment was amplified by PCR from genomic DNA with primers SJ-1632/SJ-1633. The 9,958 bp plasmid *pSJ+flank1+EF1+MIF+GFP+BAR+flank2* was used to transform Δ*Mo*MIF1-KO via ATMT, resulting in the mutant strain Δ*Mo*MIF1+GFP.

For the overexpression strain Δ*Mo*MIF1-OE_1, the *NcoI/BsrGI*-restricted plasmid *pSJ+flank1+EF1+GFP+BAR+flank2* was used as backbone for the cloning procedure. The *MoMIF1* coding sequence was amplified by PCR from genomic DNA with primers SJ-1634/SJ-1635. The 9,249 bp plasmid *pSJ+flank1+EF1+MIF+BAR+flank2* was used to transform Δ*Mo*MIF1-KO via ATMT, resulting in the mutant strain Δ*Mo*MIF1-OE_1. For the overexpression strain Δ*Mo*MIF1-OE_2, the *HindIII/NotI*-restricted plasmid *pSJ+flank1+EF1+GFP+BAR+flank2* was used as backbone for the cloning procedure. To obtain a strong expression of the *MoMIF1*-gene, the promoter of *Mo* ribosomal protein 27 was amplified from plasmid pSM565 with the primers SJ-1636/SJ-1637. The *MoMIF1* coding sequence was amplified by PCR from genomic DNA with primers SJ-1638/SJ-1639. The 8,612 bp plasmid *pSJ+flank1+RP27+MIF+BAR+flank2* was used to transform Δ*Mo*MIF1-KO via ATMT, resulting in the mutant strain Δ*Mo*MIF1-OE_2. For the reintegration of the native *MoMIF1* gene to complement the strain Δ*Mo*MIF1-KO_1, the *PstI/BglII*-restricted *pSJ-basic* was used as backbone. The NOS+BAR fragment was amplified from *pSJ+GFP(BAR)* using the primer pair SJ-1642/SJ-1643. A 1,700 bp native promoter region with the following *MoMIF1* sequence was amplified from genomic DNA with primers SJ-1708/SJ-1709. Furthermore, the C-terminal flanking region (500 bp) of *MoMIF1* was amplified by PCR from genomic DNA with primers SJ-1726/SJ-1727. The resulting 9,279 bp plasmid *pSJ+natprom+MIF+BAR+flank2 was* used to transform Δ*Mo*MIF1-KO via ATMT, resulting in the complementation strain Δ*Mo*MIF1-comp.

Protein organization comparison and phylogenetic analysis

Whole MIF and MIF domain amino acid sequences from selected species were used for the protein structure and phylogenetic analysis. Visualization and comparison of the different MIFs proteins were done via the online-tool CDD/SPARCLE (https://www.ncbi.nlm.nih.gov/Structure/cdd/wrpsb.cgi, Marchler-Bauer et al., 2017[53]). Visualization and comparison of the different MIFs domains was performed via SMART with PFAM (http://smart.embl.de; Letunic et al.[77]) Multiple sequence alignments were carried out using the MUSCLE algorithm (Edgar, 2004).[82] The phylogenetic tree was built using the maximum likelihood statistical method based on the Le's and Gascuel's model.[83] Tree nodes accuracy was tested via the bootstrap method with 1000 bootstrap replicates. Phylogenetic and molecular evolutionary analyses were conducted using MEGA software (MEGA X version 10.0.5, Kumar et al.[84]). Corresponding coding and genomic sequences were obtained from the EnsemblFungi portal (https://fungi.ensembl.org/index.html, Howe et al.[52]).

Production of sterile crude extracts from *Mo* cultures and IWF from *Mo*-infected Bd21-3 leaves

To produce new axenic cultures three agar blocks of 10 mm diameter from 11-day-old *Mo* cultures were aseptically transferred as inoculum to 200 ml liquid CM in 500 ml glass flasks with one baffle. These cultures were grown at 26°C and 120 rpm. Intercellular washing fluid (IWF) was isolated from infected leaves as described (Pogorelko et al.[85]) and followed the sequent procedure. At 2 dpi *Bd* leaves were harvested and immediately cut into 5 mm segments with a sharp razor blade and then placed into a 10 ml syringe with the tip sealed with parafilm. 5 ml of pre-chilled extraction buffer (25 mM Tris-HCl, 50 mM EDTA, 150 mM MgCl2, pH 7.4) was added, and the syringe was placed under vacuum twice for 30 min with a 5-min break. After vacuum infiltration, the buffer was carefully drained and the syringe was placed in a centrifuge tube and centrifuged at 4,000g for 10 minutes. The apoplastic fluid that accumulated at the bottom of the tube was collected in a new vial and stored on ice until assayed. All of the above steps were performed in cold storage at 4°C. Sterile solutions were obtained by filtration through disposable sterile filter (0.22 μm PES Membrane, Merck, Darmstadt, Germany). For HPLC-MS the solutions were dried with Na_2SO_4. After evaporation of the organic solvent *in vacuo* at 40°C to dryness, the residue was dissolved in methanol to give 10 mg/ml.

HPLC/MS method for analysis of secondary fungal metabolites

Crude extracts were analyzed by means of HPLC (Agilent 1100 Series) equipped with a LiChrospher RP 18 (3x125 mm; 5 μm, Merck) and a diode array detector. In order to analyse the extracts, the temperature of the column was set to 40°C and a flow rate of 1 ml/min was used with an elution gradient composed of H_2O and acetonitrile. The molecular weight of the peaks selected was determined using an HPLC-MS (Agilent 1260 Series LC and 6130 Series Quadrupole MS System). The mass spectra were recorded using atmospheric pressure chemical ionization in positive- and negative-ion mode. A Superspher RP 18 (125x2 mm; 4 μm, Merck) column was used at 40°C. For every run, 1 μl of a sample at a concentration of 1 mg/ml was injected. The elution was performed with a gradient of H_2O and acetonitrile, and a flow rate of 0.45 ml/min.

Protein purification and bottom-up proteomics analysis

The *Mo* supernatants were concentrated using tangential flow filtration (Ultrasette™ Lab Tangential Flow Device with Omega™ polyether sulfone membrane, Pall Deutschland Holding GmbH & Co. KG, Dreieich, Germany). The samples were prepared and digested before LC-MS/MS analysis as described in Ghezellou et al.[86] and Sowa et al.[87] In summary, samples were reduced and alkylated with 100 mM dithiothreitol (DTT) at 56°C for 15 min and 200 mM iodoacetamide (IAA) at room temperature (dark place) for 30 min, respectively. The digestion was performed with a mass spec grade Trypsin/Lys-C mix (1:50 enzyme to proteins ratio; Promega GmbH, Mannheim, Germany) overnight.

The resulting peptides were separated by UltiMate 3000 RSLC UHPLC system (Thermo Fischer Scientific, Bremen, Germany) equipped with a Kinetix C18 column (Phenomenex, 2.6 μm, 100 Å, inner diameter 2.1 mm, 100 mm length) coupled with a Q Exactive HF-X Orbitrap (Thermo Fischer Scientific) mass spectrometer. Chromatographic analysis was performed at a flow rate of 250 μL min-1 with water/0.1% formic acid (mobile phase A) and acetonitrile/0.1% formic acid (mobile phase B). The gradient elution of 80 min was performed as follows: 2% B for 5 min, followed by 2–40% B over 60 min, 40–50% B over 5 min, 50–98% B over 5 min, and re-equilibration in 2% B. The mass spectrometer was operated in data-dependent acquisition (top-10 DDA) with the following parameters in full MS scans: a mass range of m/z 350–1800, mass resolution of 120,000 (@ *m/z* 200), AGC target of 3e6, injection time (IT) of 50 ms, and MS/MS scans: mass resolution of 30,000 (@ *m/z* 200), AGC target of 1e5, IT of 120 ms, isolation window *m/z* ±1.3, dynamic exclusion of 30 s and normalized collision energy (NCE) of 28. The raw files were processed using Proteome Discoverer version 2.4 (Thermo Scientific) with SEQUEST and MS Amanda search engines against the MIF databases.

Vegetative growth assays

Stress tolerance of mutant strains was conducted according to Jacob et al.[88] Agar blocks of approximately 0.8 cm diameter from 11-day-old *Mo* cultures grown on CM were cut out to be tested and transferred on CM or MM agar plates with different stress-inducing compounds (sorbitol, KCl, NaCl). The cultures were grown for 7 days at 26°C.

Appressorium formation assays and conidia morphology

Appressorium development was assayed by monitoring germination of conidia on hydrophobic plastic slides (thickness 1, 76x51 mm, no. 653081; Greiner BioOne, Kremsmünster, Austria). For this purpose, conidia were harvested from 12-day-old *Mo* cultures grown on CM,

filtered through two layers of miracloth to give a conidial suspension, which was adjusted to 5 x 10^4 conidia mL^{-1} in ddH_2O. 100 µl drops of this conidial suspension were placed on the plastic slides and incubated at room temperature. After 16 h the number of appressoria formed was counted. In addition, the same assay was carried out on glass slides upon chemical stimulation with 500 ng mL^{-1} 1,16-hexadecandiol (1,16-HDD, dissolved in MeOH). 1,16-HDD is a plant lipid or wax compound and an inducer of appressorium formation in *Mo*.[89]

For the cytorrhysis assay, different concentrations of glycerol (1 M, 2 M, 3 M, 4 M) were added to the differentiated appressoria and after 5 min the number of collapsed appressoria was counted.

Confocal laser scanning microscopy

Images were taken using a Leica TCS SP8 confocal laser scanning microscope (CLSM, Wetzlar, Germany) equipped with a 75-mW argon/krypton laser (Omnichrome, Chino, CA) and a water immersion objective (HCX APO L40x0.80 W U-V-I objective). Images were processed using the Leica LAS X software. GFP: green fluorescence ($\lambda_{emission}$: 508 nm; $\lambda_{excitation}$: 489 nm).

Transient expression in *N. benthamiana*

For transient expression analysis, *A. tumefaciens* GV3101 strains containing constructs with genes encoding either *Mo*MIF, mBAX, and GFP were grown in LB medium supplemented with 50 µg/mL rifampicin, 20 µg/mL gentamicin and 100 µg/mL spectinomycin until OD_{600} reached 1.0. Cells were pelleted, resuspended in infiltration buffer (10 mM $MgCl_2$, 10 mM 2-[N-morpholino] ethanesulfonic acid [MES], pH 5.6, 200 µM acetosyringone) and adjusted to an OD_{600} of 0.6, then left for 3h at room temperature. The solutions were combined such that the final OD_{600} in the mixtures were 0.375 for *MoMIF-*, 0.125 for *GFP-*, and 0.05 for *mBAX*-containing agrobacteria. The abaxial side of leaves from 4-week-old *N. benthamiana* was infiltrated using a syringe without a needle. The leaves were scored for cell death 48 h after infiltration. For subcellular localization studies, *Mo*MIF1 was tagged at the N-terminus with eGFP (plasmid pK7WGF2) and transferred into Agrobacterium strain GV3101. The bacterium was grown as described above and infiltrated into *N. benthamiana* leaves at on OD_{600} of 0.5. Leaf patches were analyzed by CLSM 48 h after infiltration on an inverted Zeiss LSM880 microscope (Carl Zeiss France SAS, Marly-le-Roi, France), equipped with Argon ion and HeNe lasers as excitation sources. Samples were excited at 488 nm and images were acquired with a C-Apochromat 63x/1.20 W Corr M27 objective and processed using the Zeiss ZEN 2 software package.

QUANTIFICATION AND STATISTICAL ANALYSIS

DNA/RNA isolation and quantitative PCR and RT-PCR analysis

DNA was extracted from roots and leaves using a DNA extraction kit (Qiagen) according to the manufacturer's instructions, and quantification of *Mo* DNA presence was assessed by quantitative PCR based on the ratio of the fungal *actin* (*MoActin*) or *glyceraldehyde-3-phosphate dehydrogenase* (*MoGPD*) normalized to *Bd ubiquitin* (*BdUbiquitin*) in the QuantStudio 5 Real-Time PCR system (Applied Biosystems, see below).

RNA extractions, DNase treatment, cDNA synthesis and quantitative RT-qPCR were performed as described in Kumar et al.[90] In summary, RNA extraction was performed using GENEzol reagent (Geneaid) according to the manufacturer's instructions. DNA was subsequently digested with DNAse I (Thermo Scientific) according to the manufacturer's protocol and the remaining RNA was used for cDNA synthesis using the qScript™ cDNA kit (Quantabio). For RT-qPCR, 10 ng of cDNA was used as starting template in the QuantStudio 5 Real-Time PCR system (Applied Biosystems). Ct values were determined using the QuantStudio design and analysis software included with the instrument. Transcript amounts were determined using the $2^{-\Delta\Delta Ct}$ method by normalizing the amount of the target transcript to the amount of the reference transcript *actin* (*MoActin*) or *glyceraldehyde-3-phosphate dehydrogenase* (*MoGPD*) genes. Primer pairs used for PCR and expression analysis are listed in Table S1.

Statistical analysis

Student's t-test, ANOVA test with Pairwise Comparisons with Bonferroni adjustment, ANOVA with posthoc Tukey HSD test or Kruskal Wallis followed by pairwise adjusted with Benjamin-Hochberg correction for multiple comparisons or Dunn's test were selected after analysis of the sample distribution in the different groups. Statistical details of each experiment can be found in the final section of the figure legends. Figure legends include the statistical tests used, exact value of samples used for the test analysis (n) and dispersion and precision measures (standard deviation (±SD) of three or more biological repetitions).